Nanosized tubular clay minerals as inorganic nanoreactors for energy and environmental applications: A review to fill current knowledge gaps

Yassine Naciri, Mohamed Nawfal Ghazzal, Erwan Paineau

Nanosized tubular clay minerals as inorganic nanoreactors for energy and environmental applications: A review to fill current knowledge gaps

Yassine Naciri[1,2], Mohamed Nawfal Ghazzal[2,*] and Erwan Paineau[1,*]

[1]Université Paris-Saclay, CNRS, Laboratoire de Physique des Solides, 91405 Orsay, France

[2]Université Paris-Saclay, CNRS, UMR8000, Institut de Chimie Physique, 91405, Orsay, France.

* mohamed-nawfal.ghazzal@universite-saclay.fr; erwan-nicolas.paineau@universite-paris-saclay.fr

Abstract

Modern society pays further and further attention to environmental protection and the promotion of sustainable energy solutions. Heterogeneous photocatalysis is widely recognized as one of the most economically viable and ecologically sound technologies to combat environmental pollution and the global energy crisis. One challenge is finding a suitable photocatalytic material for an efficient process. Inorganic nanotubes have garnered attention as potential candidates due to their optoelectronic properties, which differ from their bulk equivalents. Among them, clay nanotubes (halloysite, imogolite, and chrysotile) are attracting renewed interest for photocatalysis applications thanks to their low production costs, their unique physical and chemical properties, and the possibility to functionalize or dope their structure to enhance charge-carriers separation into their structure. In this review, we provide new insights into the potential of these inorganic nanotubes in photocatalysis. We first discuss the structural and morphological features of clay nanotubes. Applications of photocatalysts based on clay nanotubes across a range of photocatalytic reactions, including the decomposition of organic pollutants, elimination of NOx, production of hydrogen, and disinfection of bacteria, are discussed. Finally, we highlight the obstacles and outline potential avenues for advancing the current photocatalytic system based on clay nanotubes. Our aim is that this review can offer researchers new opportunities to advance further research in the field of clay nanotubes-based photocatalysis with other vital applications in the future.

Keywords: Photocatalyst; clay nanotubes; imogolite; halloysite; chrysotile.

Introduction

The hasty growth of the global economy and industrialization over the past century has also led to severe problems worldwide. The world's reserve of natural energy is expected to be depleted within the next 50 years [1]. Experts consider global warming and climate change to be a direct consequence of the exponential increase in the consumption of fossil fuels. The increase in industrial pollutants is another consequence of the extensive use of these resources [2–4]. Requirement for developing environmentally friendly and energy-conserving solutions to address environmental remediation.

Solar energy represents a highly promising resource due to its unique advantages. It offers an abundant and inexhaustible source of power, surpassing global energy consumption by several times [5–7]. Furthermore, solar energy is environmentally friendly, emitting minimal greenhouse gases, thereby helping to mitigate climate change. According to United Nations Development Programme data, the annual solar energy potential ranges from 1575 to 49387 exajoules (EJ) [8], which greatly exceeds our global annual energy consumption of 559.8 EJ. This remarkable surplus makes solar energy a viable and sustainable solution for driving human development. Numerous fields use solar energy, such as photovoltaics, thermal energy, artificial photosynthesis, solar architecture, and photocatalysis [9–13]. Among them, photocatalysis emerges as a cutting-edge method for harnessing sunlight and expediting molecular conversions to generate solar-derived fuels, primarily hydrogen (H_2), paving the way to a clean and renewable energy source [14,15].

In photocatalysis applications, the extensively used photocatalysts such as TiO_2 and ZnO face two primary challenges [16–19]. They have a limited spectral response interval, only capturing a minor portion of the solar spectrum (less than 5%), confined to the UV region [4,20]. Additionally, their high charge carrier recombination leads to poor quantum yield [21–25]. As a result, researchers are exploring alternative materials to overcome these limitations. Recent focus has been on 1D nanostructures, whose unique properties hold promise for enhancing photocatalytic activity and expanding its applications.

Since the emergence of carbon (C) nanotubes (NTs) at the beginning of the ’90s [26], a considerable part of the literature has focused on applying one-dimensional (1D) tubular nanomaterials in numerous fields, including photocatalysis [27–29]. Carbon nanotubes and their inorganic (oxides, sulfides…) analogs have distinctive electronic characteristics such as exceptional electron mobility, the quantum confinement effect, and an extraordinarily large specific surface area [30–32]. The reverse movement of holes and electrons can be promoted by the existence of polarization within the photocatalytic material [33–35]. Numerous studies have reported that the tubular structure led to improved properties. Among them, titania nanotubes exhibited enhanced photocatalytic activity compared to other titania structures [36,37]. Thus, targeting photocatalysts with tubular structures should result in enhanced photocatalytic performance.

Although carbon is probably the most studied nanotube material [38–40], various nanotube materials, such as natural clays, have garnered significant interest because of their intriguing characteristics and attributes [41–44]. When referring to clay minerals (or phyllosilicate), we mostly talk about low-dimensional 2D nanostructures. However, clay minerals can adopt also 1D tubular structures.The

importance of tubular clay materials as a substituent for expensive CNTs and other nanomaterials is universally recognized [45,46]. Hydrosilicates are considered the most promising nanotube clays minerals due to their ability to scroll spontaneously: chrysotile ($Mg_3Si_2O_5(OH)_4$) [47], halloysite ($Al_2Si_2O_5(OH)_4$) [48–50] and imogolite ($Al_2SiO_3(OH)_4$) [51–54]. The crystal structures of imogolite and halloysite combine an aluminum-oxygen dioctahedral sheet covalently bonded to a silicon-oxygen tetrahedra layer for halloysite or to isolated silicon-oxygen tetrahedral in the case of imogolite. For chrysotile, the sheet is classified as trioctahedral as it is mainly composed of magnesium [55]. The differences in the size of sheets and structure led to a bending momentum, transforming the layers into single-walled or multi-walled tubular [56–58]. Additionally, it's worth noting that the unique bending energy of these nanotubes is a key factor in their remarkable stability and mechanical properties, with a Young modulus around approximately 150 GPa for chrysotile [59], 140 GPa for halloysite [60], and between 200-600 GPa for imogolite [61]. Recent research on imogolite nanotubes and hydroxyl vacancies in aluminosilicate and aluminogermanate nanotubes has further highlighted the significance of bending energy in influencing their overall mechanical behavior [57,58]. Understanding the bending energy of these nanotubes opens up exciting possibilities for tailored applications in various scientific and engineering fields.

Due to their unique properties (e.g., improved light scattering and harvesting, shorter distances for charge transfer, and direct charge separation), materials with a tubular structure have recently found potential in the photocatalysis field [62]. Consequently, tubular clay minerals such as imogolite, chrysotile, and halloysite hold the potential to be used, in principle, for such applications. The energy gaps of these nanotubes vary between 4.2 eV to 5.2 eV [63,64], which refers to the minimum

energy to excite and separate an electron (e^-) and a hole (h^+) toward the conduction and valence bands, respectively. Additionally, the 1D structure facilitated the effective diffusion of photogenerated electrons and holes [65]. For imogolite nanotubes, recent theoretical investigations have revealed that the curvature of the nanotube wall generates an electronic density distribution and increases the internal electric field, which causes a static force and facilitates the separation of electron-hole pairs [65,66]. Thus, the synergy between polarization and the one-dimensional structure of these photocatalysts is beneficial, as it can enhance the spatial separation of the charge carriers.

These clay materials (imogolite, chrysotile, and halloysite) can also be applied as support materials or in conjunction with other photocatalysts to improve the performance of the hybrid structures in degrading numerous pollutants [47,67,68]. The improved photocatalytic efficiency results from the synergistic interaction of the unique characteristics of these clay materials, such as their exceptional light absorption, large specific surface area, and visible light absorption ability. It was noted that the halloysite was used in broader applications than the chrysolite and imogolite. This is due to the advantageous attributes of halloysite, such as its affordability and low toxicity, which surpass those of chrysolite [69]. While imogolite is not produced in large quantities yet their efficiency is greater than halloysite. The increasing fascination with halloysite is evident in the rising count of scientific publications and patents over the past decade (**Fig.1**).

As far as we know, this review is the first attempt to thoroughly examine recent advances in synthesizing and applying nanosized tubular clay, specifically halloysites, chrysolite and imogolites, as true photocatalysts, or in combination with other semiconductors for heterogeneous photocatalysis, with a particular focus on

their properties for energy and environmental applications. After a brief preamble on the principles of photocatalysis, we focus on analyzing the synthesis, structural, physiochemical properties, and photocatalytic activity of clay nanotubes (imogolite nanotubes (INTs), halloysite nanotubes (HNTs) and chrysolite (CINTs)). We introduce the significance of using nanotube architectures in photocatalysis and discuss the polarization effect's role. This review subsequently addresses the processes that improve photocatalyst performance when combined with tubular clay. Lastly, research opportunities for tubular clay photocatalyst material are proposed.

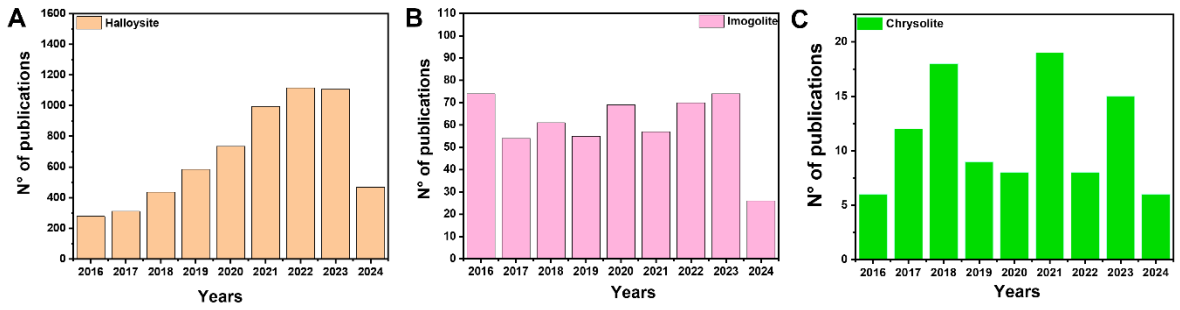

Fig.1. Yearly scientific publications and patents on **A**) halloysite, **B**) imogolite and **C**) chrysolite nanotubes. The data displays the last decade (Data from the "Web of Science").

2. Semiconductor photocatalysis: General principles and mechanism

Photocatalytic reactions are regarded as one of the most effective methods for harnessing solar power. In addition to the established techniques of generating solar fuels by splitting water and reducing carbon dioxide, photocatalysis has found applications across a wide range of fields [27,67,70–73], varying from pollutant degradation to fine chemical production (**Fig.2A**) [74].

Generally, the photocatalysis downhill thermodynamics (Gibbs free energy change $\Delta G<0$) is purely enhanced by the induced reactive oxygen species (ROS) from the photocatalysts' excitation under light irradiation (**Fig.2B**) [75]. However, the unfavorable

photosynthesis reaction (ΔG>0), an uphill reaction, is primarily determined by photogenerated holes and electrons characterized by high redox potentials (**Fig.2B**) that need to be assured by the correct positioning of the conduction and valence bands [76]. From a thermodynamic point of view, photocatalytic degradation is much more feasible than the challenging artificial photosynthesis processes, such as photocatalytic hydrogen (H_2) evolution and the production of hydrocarbon fuels from carbon dioxide (CO_2) reduction.

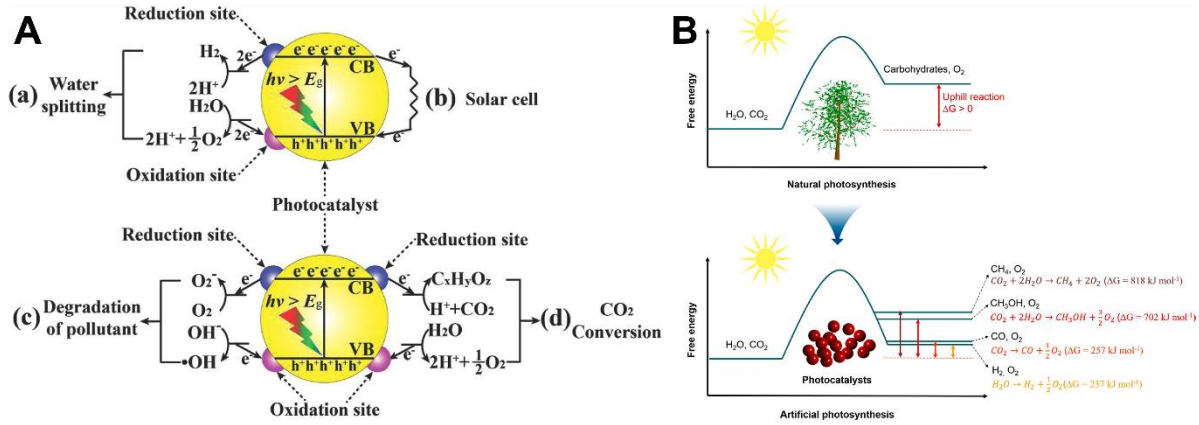

Fig. 2. A) Water splitting, solar cell, pollutants photocatalytic degradation, and photocatalytic reduction of CO_2 mechanisms. Adapted with permission from [74], Copyright (2014), Wiley. **B**) Schematic illustration of natural and artificial photosynthetic systems [77], Copyright (2019), American Chemical Society.

Fig.3A displays the redox mechanism for semiconductors (SCs) used as photocatalysts. The mechanism involves three successive steps [78,79]. Initially, the SC photocatalyst absorbs photons, and this causes electrons (e^-) in the valence band (VB) to jump to the conduction band (CB) when the photon energy (hv) exceeds the bandgap energy (Eg) of the semiconductor. Consequently, holes (h^+) are left behind in the VB. These electrons and holes are crucial in driving reduction and oxidation reactions to yield the desired product [79]. The subsequent step involves separating and transferring photogenerated electron-hole pairs, directing them toward the semiconductor's surface, although some of these pairs may

recombine within the bulk of the photocatalyst [80]. The last step comprises surface-based reduction and oxidation reactions. The photogenerated charges located on the surface of the semiconductor engage with chemical species, thus initiating the desired chemical reactions. However, on the surface, certain photogenerated electrons (e^-) and holes (h^+) may recombine without actively engaging in chemical reactions. **Fig.3B** displays a schematic representation of the time scale characteristics associated with the various phenomena related to charge carriers that were previously discussed [81].

With the modern insight into the photocatalytic mechanisms, enhancing the effectiveness of semiconductor photocatalysts involves expediting the production, mobility, and reactivity of photo-induced charge carriers while minimizing electron-hole recombination. Semiconductor materials with suitable bandgap structures for solar light absorption, efficient conductivity for charge transport, minimal defects as recombination sites, and rapid kinetics for surface reactions are highly favored [82,83]. In general, for the reaction to proceed effectively, the reduction potential should be lower than the bottom edge of the semiconductor's conduction band (CB), enabling the transfer of electrons from the CB to the reactant. Furthermore, the oxidation potential must exceed the VB of the catalyst to ensure the reactant can readily accept holes.

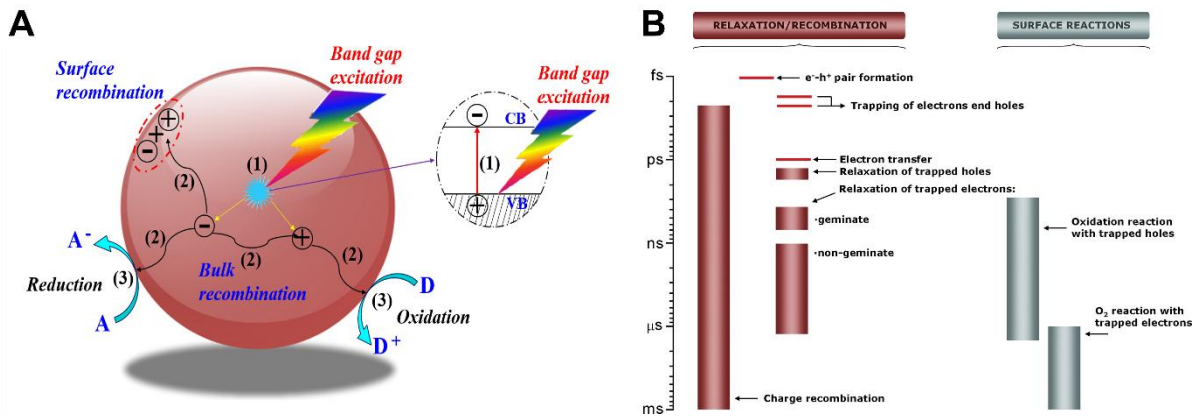

Fig. 3. **A**) Schematic diagram illustrating principle of photocatalyst photocatalysis. **B**) Time intervals between "elementary steps" in a typical photocatalytic reaction. Adapted with permission from [81], Copyright (2012), American Chemical Society.

Adsorption plays a pivotal role in heterogeneous photocatalysis [84–86], particularly in the degradation and transformation of organic molecules or gases, where clay catalysts have emerged as significant contributors. Clay minerals, with their abundant surface area and reactive sites, offer a favorable environment for adsorption and catalytic processes [50,53,87]. Organic molecules or gas reactants adhere to the surface or interlayer spaces of clay catalysts through electrostatic interactions and other surface phenomena, initiating photocatalytic reactions. The subsequent generation of superoxide and hydroxyl radicals facilitates the breakdown of adsorbed molecules, leading to the desired transformations [88,89]. Despite the essential role of adsorption, competitive interactions among water molecules, other reactants, and target molecules may influence the photocatalytic efficiency, impacting active site availability and photogenerated species migration. While adsorption enhances catalytic efficiency by promoting reactant-catalyst interactions, excessive adsorption of certain compounds or intermediates can impede the process by acting as catalyst poisons [90]. Nonetheless, adsorption serves as the initial step in catalysis, concentrating reactants near active sites, and reducing the activation energy required for chemical transformations to occur. The versatility of clay catalysts allows for tailored surface properties and selective adsorption, enabling the direction of reactions toward desired pathways and improving overall process performance in terms of reaction rates, selectivity, and yield for various organic molecules or gas reactants [89].

Recently, several studies demonstrated that tube morphology is one of the crucial parameters that can significantly influence the performance of the

photocatalyst [27,91,92]. In particular, there is compelling evidence that materials featuring nanotubes display improved photocatalytic activity compared to nanoparticles. Moreover, materials with tubular structures have been reported to exhibit much better photocatalytic performance than nanoparticulate systems. For instance, a study by Jiang et al [93] demonstrated that halloysite exhibits superior photocatalytic activity in photodegradation processes of different organic contaminents (rhodamine B, malachite green and ciprofloxacin) compared to their 2D polymorph (kaolinite nanosheets). Their results highlight the enhancement of photocatalytic activity due to the tubular morphology of halloysite. The extended axis of nanotube photocatalysts provides a straight path for carrier transport [94], thus lowering photoinduced electron-hole pairs' trapping and recombination kinetics [95]. This compares sharply with the transporting of the electron-hole pairs between nanoparticles. Moreover, nanotubes can provide a strong light-scattering effect, improving the light-harvesting properties [94]. Additionally, polarization can improve charge separation within a photocatalyst material by facilitating the movement of electrons and holes in opposite directions [96]. The nanotubes' geometry reduces the diffusion distance between the degrading compounds in the solution and the nanotubes' active surface area. Whereas the porous structure of nanoparticles imparts longer diffusion lengths [95]. These advantages can be applied to nanosized tubular clay minerals (halloysite, imogolite, and chrysotile). **Fig. 4A and Fig. 4B** outline the electron transport in two distinct architectures of the photocatalyst and schematic illustrations of some pros of nanotubular architecture for photocatalytic reaction, respectively.

We can summarize and highlight the action mechanism of clay nanotubes in altering photocatalytic properties as follows: The tubular architecture of these clay

variants provides a confined environment that boosts the efficiency of photocatalytic reactions by facilitating the adsorption of reactant molecules and promotes proximity to active sites and catalytic centers [93,97]. Additionally, the high surface area-to-volume ratio of clay nanotubes allows for increased contact between catalysts and reactants, enhancing reaction kinetics [93]. Moreover, their structural characteristics enable efficient light harvesting and photon utilization, while surface chemistry facilitates charge transfer processes crucial in photocatalytic reactions [98,99]. The polarization effect within tubular clay minerals further aligns molecules and charge carriers, streamlining charge transfer and reducing recombination rates, thus amplifying overall photocatalytic activity [100,101].

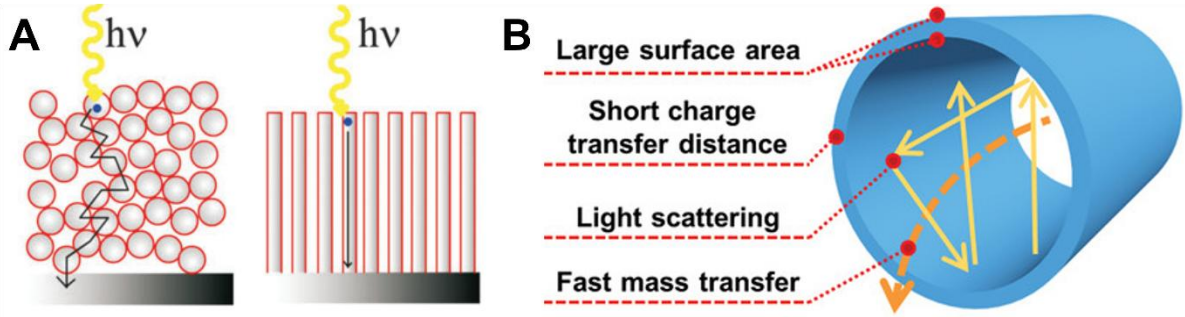

Fig. 4. A) A comparison of the electron pathways through nanoparticle and nanotubular structured TiO_2. Reproduced with permission from [102], Copyright (2009). The Royal Society of Chemistry. **B)** Schematic illustration of some advantages of nanotubular architecture for photocatalytic reactions. Reproduced with permission from [103], Copyright (2019) Wiley.

3. Structural and physiochemical properties of the nanosized tubular clay minerals.

Compared to other nanomaterials with spherical or platy shapes, nanotubes, such as chrysotile, halloysite, and imogolite, offer a larger surface area due to their unique hollow tubular structure [104]. In the following discussion, we will examine the detailed aspects of these nanosized tubular clay minerals, exploring their

composition, structure, and exceptional physiochemical properties that distinguish them in materials science.

3.1. Structural and physiochemical properties of Halloysite

Halloysite nanotubes (HNTs) represent an exciting source of 1D clay material that can be extracted in large quantities from deposits, making them economically viable. The most widely available halloysite supplies are from Dragon Mine (Utah-USA) and Northland (New Zealand) deposits [105,106]. Due to its distinctive tubular nanostructure, HNTs has garnered significant attention across various fields in recent years. Its applications range from controlled release of functional compounds, anticorrosion, adsorbents, catalysis supports and nanotemplate/nanoreactor [93,97,107–110].

Halloysite is a dioctahedral 1:1 clay mineral with a chemical formula of $Al_2(OH)_4Si_2O_5.nH_2O$, belonging to the kaolin group with a nanoscroll shape formed by rolling 5-20 aluminosilicate layers [111,112] (**Fig. 5A)**. When *n* = 2, halloysite is referred to as halloysite-10 Å due to the average spacing of 10 Å between the unit layers. Water can be removed almost permanently by heating the halloysite samples at 120 °C, leading to halloysite-7 Å (with an interlayer spacing of 7Å) [87]. The structure of halloysite is known as monoclinic with unit cell parameters as follows: a = 5.14, b = 8.9, c = 17.7 Å with angles α ranging from 97 to 104 degrees, β from 90 to 91.8 degrees, and γ fixed at 90 degrees. The halloysite is characterized by a hollow spiral structure [113] as illustrated by images using AFM and TEM techniques (**Fig. 5B)**. The length of HNTs ranges typically within 0.5-1.5 μm [111,112]. The outer

diameter ranges between 50 to 70 nm, while the inner cavity, also called lumen, has a 10 to 20 nm diameter. In addition, halloysite exhibits distinct internal and external chemistry. The inner lumen surface features an array of Al-OH groups resembling gibbsite and carries a positive charge, whereas the outer surface consists of Si−O−Si groups and bears a negative charge [41]. This characteristic of a different surface charge outside and inside the tube makes the incorporation of ligands and nanomaterials feasible in the desired location. Joo *et al.* [114] observed that changing the pH in a water suspension containing HNTs allowed the tailoring of the pore surface area, pore diameter, and pore volume of the recovered halloysite powder (**Fig. 5C**). Indeed, in an acidic solution, bundles of halloysite nanotubes are formed (blocking the halloysite nanotube inner pore). In contrast, HNTs are well dispersed in basic solution, and the end of each HNTs was separated from other HNTs. An important point it that the synthesis of halloysite remains an ongoing challenge due to the absence of well-established procedures. Research efforts in this area have been underway since the mid-20th century. However, to date, developing a reliable and efficient method for synthesizing halloysite in the laboratory continues to be an urgent and unresolved issue [115].

Continuing the research on the properties of the HNTs, Gianni et al [116]. conducted a comprehensive theoretical study using DFT calculations to examine the electronic characteristics of halloysite nanotube models (**Fig. 5D**). Their study revealed that the pristine halloysite nanotube exhibits a band gap of 5.14 eV (**Fig. 5E**). Through the analysis of the total density of states (TDOS) and projected density of states (PDOS) of halloysite, they highlighted that the lower and upper sections of the valence band consist primarily of oxygen 2s and oxygen 2p states, respectively. The oxygen atoms forming Al-O bonds significantly contribute to the valence band

compared to those involved in Si-O bonds [116,117]. The conduction band minimum primarily comprises H 1s, Si 3s 3p, and partly O 2p, Al 3s 3p states. The same calculations were confirmed by independent researchers [116,117].

The hollow structure of HNT acts as a nanoreactor, providing a confined environment that enhances the effectiveness of catalysts. Recently, Jiang and colleagues [93] investigated the use of natural HNT as a nanoreactor to improve photochemical reactions. Their research demonstrated that introducing Fe doping into the interior surface of HNT resulted in enhanced activity and adsorption capabilities compared to the exterior surface. Notably, the unique photochemical properties exhibited by the two surfaces of HNT led to spatial confinement effects, resulting in superior photodegradation of organic species compared to kaolinite nanosheets.

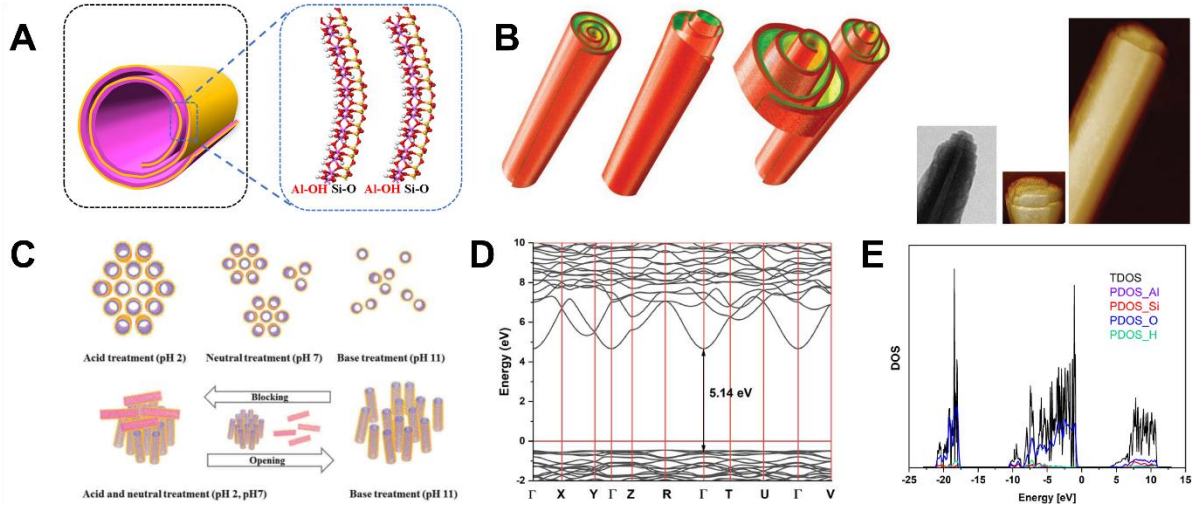

Fig. 5. **A**) Detailed structure of halloysite nanotubes. Reproduced with permission [93]. Copyright (2021), American Chemical Society. **B**) Scheme of the rolling of alumosilicate sheets to create halloysite nanotubes, with alumina forming on the interior (green), silica on the outside and representative TEM and AFM images of HNTs. Reproduced with permission from [41]. Copyright (2015), Wiley. **C**) Schematic representation of the inner space of halloysite nanotubes and the inter-space between them following treatment with various pH solutions. Reproduced with permission from [114], Copyright (2013), Royal Society of Chemistry. **D**) The calculated band gaps for and **E**): The calculated TDOS and PDOS of respective

atoms for the the halloysite. Reproduced with permission from [116] Copyright (2023), Elsevier.

3.2. Structural and physiochemical properties of imogolite

Yoshinaga and Aomine first discovered imogolite (INT) from volcanic ash in 1962. INT is a naturally occurring aluminosilicate nanotube [118], characterized by the chemical formula $(OH)_3Al_2O_3SiOH$, extending from the outer to the inner surface of these nanotubes [53,119]. This particular nanotube features an inner and outer diameter of about 1.0 nanometers and approximately 2 nanometers, respectively [54], while the length varies from hundreds of nanometres to the micrometer scale (**Fig. 6A).** The interior of imogolite exhibits silanol (SiOH) groups, while the exterior showcases both Al–O–Al and Al–OH–Al groups, providing imogolite nanotubes with amphoteric properties [120]. The spontaneous rolling of an Al-O and Si-O bond into a single-walled nanotube is caused by the difference in bond length. More interestingly, these configurations exhibit a clearly defined minimum in strain energy [57,58,121], facilitating monodispersity in nanotube diameter and chirality [122]. It is worth highlighting that the structure of imogolite differs significantly from that of halloysite. In imogolite, the curved octahedral $[Al(OH)_3]$ layer shapes the inner surface of the nanotubes, whereas the outer surface is composed by Si-O-Si group [53]. These distinctions are at the core of the unique characteristics of imogolite nanotubes. Moreover, INTs are often regarded as the clay equivalent of carbon nanotubes, exhibiting remarkable resemblances in aspect ratios, rigidity, and dimensions [112].

The major limitation of INTs, from an industrial point of view, is their inability to create extensive deposits [123]. However, its synthesis was established quite rapidly after its discovery. In 1977, for the first time, Farmer et al. [124] synthesized

imogolite nanotubes by coprecipitating silicon and aluminum in an aqueous solution. They established that the yield and rate of formation of imogolite nanotubes are optimal for (i) a pH of 4.5, (ii) low reactant concentrations, and (iii) a temperature between 90 and 100 ˚C [125].

The electronic characteristics of INTs depend on their diameter, chemical composition, and chirality. An indicator of a promising photocatalyst is its band gap. Bursill et al. [126] were the first to predict a relatively wide band gap for these nanotubes. Subsequent band gap values for imogolite nanotubes have been shown to range from 3.6 to 5.3 eV [57,58,64,127,128]. Moreover, Li and co-workers [127] demonstrated that the structure of the energy band and the electron density of states were near the Fermi level (set at E= 0) for a single-walled imogolite (**Fig. 6B**). Their findings indicated a direct band gap with an E_g of approximately 3.67 eV. Moreover, the energy gap shown in the DOS (**Fig. 6B**) corresponds to the energy band gap shown in **Fig. 6C.**

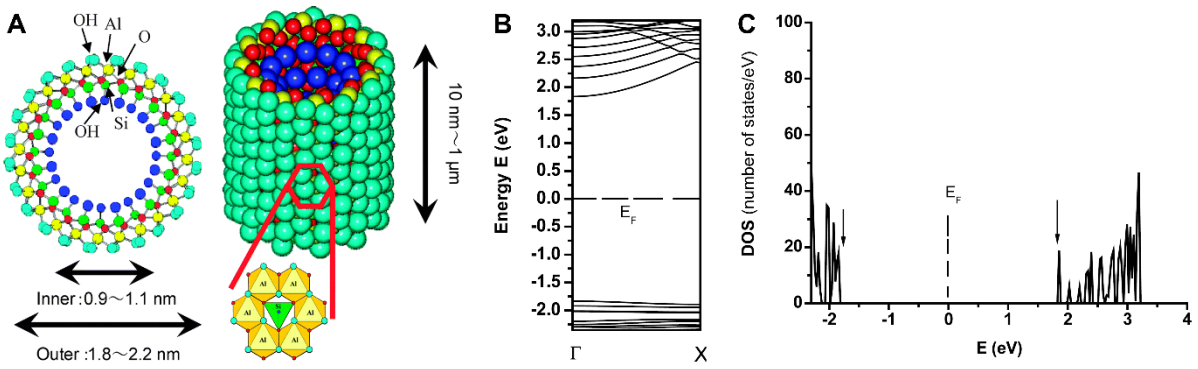

Fig. 6. **A**) Structural illustration of imogolite. Reproduced with permission from [129], Copyright (2014), Royal Society of Chemistry. **B**) The energy bands of the single-walled imogolite nanotube and **C**) the electron density of states. Reproduced with permission from [127] .Copyright (2008), IOP Publishing.

3.2.1. Synthesis and physiochemical properties of compounds analogous to imogolites

Chemically tuning synthetic materials primarily aims to expand the range of potential industrial applications. Similarly, synthetic procedures often allow for better control over reproducibility, composition, purity, and specific desired characteristics, unlike natural clay specimens, which frequently contain impurities and can be less readily available. Notably, in the case of nanotubular structures, it is essential to establish practical approaches for controlling the functionality of both their inner and outer surfaces.

Wada and co-workers successfully substituted the silicon atoms with germanium in the imogolite structure by modifying the precursors of the synthesis [130]: By using electron microscopy and X-ray scattering analysis, they found that the diameter of imogolite nanotubes increases as the [Ge]/([Ge]+[Si]) ratio increases. Conversely, they also observed a reduction in the length of the tubes with the increase in this substitution rate. It's worth mentioning that by replacing NaOH with urea in the synthesis procedure, some researchers substantially increased the length of Ge tubes [131,132]. However, Maillet et al. [133] observed in their study that the nanotube shape is regulated by the initial aluminum salt (C_{Al}) concentration, generating either single-walled nanotubes (Ge-SWINT, $C_{Al} > 0.75$ mol L^{-1}) or double-walled (Ge-DWINT, $C_{Al} < 0.4$ mol L^{-1}) (**Fig. 7A**) [53]. These structures (Ge-SWINT and Ge-DWINT) have been thoroughly investigated through experimental and computational studies [65]. The results of this study proved that the Ge-DWINT structure exhibits more excellent stability compared to Ge-SWINT, possibly attributable to hydrogen bonding stabilization. It has also been deduced that while aluminosilicate nanotubes exhibit insulating properties, their dehydroxylation can alter them into semiconductor materials [133]. On the other hand, Alvarez-Ramirez

[128] performed ab initio simulations, from which they estimated a band gap range of 4.3-4.8 eV for Ge-Imo.

Surface modification has also been applied to Imogolite nanotubes. Bottero et al. [134] were the first to report the synthesis of silicon-based imogolite with a fully methylated inner wall (**Fig. 7B**) [135]. A few years later, the technique was successfully transposed to germanium imogolite nanotubes (**Fig. 7C**) [136,137]. It was worth mentioning that the methylation of imogolite nanotubes was confirmed to induce a significant increase in their affinity with molecules such as CH_4, CO_2, or N_2 [138]. Curiously, Pignié et al. [100] recently reported that the imogolite IMO-CH_3 (5.4 ± 0.2) has a smaller energy gap than the pure imogolite IMO-OH (5.85 ± 0.30) (**Fig. 7D)**. This value is similar to the band gap related to ZrO_2 (**Fig. 7E**), whose photocatalytic activity has been extensively studied. Given the similarity in band gaps and valence/conduction bands between ZnO_2 and imogolite variants (IMO-CH_3 and MO-OH) [100] and the successful use of ZnO_2 in harnessing solar energy [139–141], it suggests imogolite holds promise as a viable candidate for effective photocatalytic applications. Furthermore, the versatility of imogolite nanotube functionalization opens exciting opportunities in the field of photocatalysis.

Finally, focused on these encouraging findings, other isomorphic substitutions have been studied lately, especially regarding the partial replacement of Al^{3+} with Fe^{3+} in the outer wall [142–144]. Despite these enhancements, they do not substantially alter the nanotube diameter, with doping rates remaining below 1% [142]. Alvarez-Ramírez's work has shown that the incorporation of Fe alters the electronic characteristics of the nanotubes, consequently causing the band gap value to decrease. This decrease is observed from 4.7 eV to 2.0-1.4 eV for the Fe-silicon nanotubes and from 4.2 eV to 2.6-1.0 eV for the Fe-germanium imogolite-like

nanotube [63]. "In addition to iron substitution, other trivalent dopants or cation vacancies have been theoretically contemplated, which have the potential to bring about substantial alterations in the band structure of these nanotubes [145–148]. Therefore, these different perspectives on the optical and electronic properties of modified imogolite nanotubes open the way to their practical use as a photochemical nano-reactor.

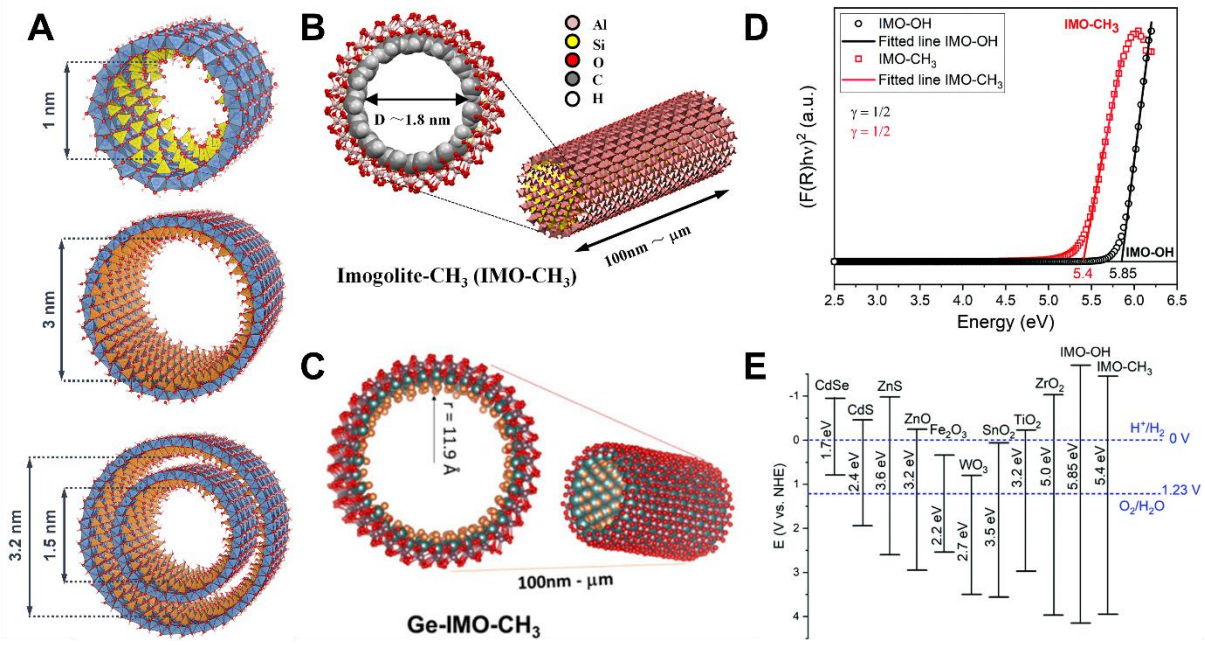

Fig. 7. Inner diameter size for **A**) Si-SWINT, Ge-SWINT and Ge-DWINT. Reproduced with permission from [53], Copyright (2018) MDPI. **B**) Methylated imogolite (IMO-CH_3). Reproduced with permission from [137], Copyright (2017) Elsevier. **C**) SW Ge-IMO-CH_3. Reproduced with permission from [135], Copyright (2019) American Chemical Society. **D**) Band gap energy of IMO-OH and IMO-CH_3 and **E**) Comparison of the gap band of the imogolite with other selected compounds. Reproduced with permission from [100], Copyright (2021) Royal Society of Chemistry.

3.2.2. The role of polarization of imogolite in photocatalysis

As mentioned, a fundamental challenge in photocatalysis lies in rapidly recombining electron-hole pairs within photocatalysts. While the charge migration

458 requires hundreds of ps, bulk charge recombination occurs much faster, taking only
459 a few ps. which is considerably swifter than charge transport [149]. For that reason,
460 Therefore, suppressing the process of electron-hole pairs recombining (e^-/h^+) stands
461 as a crucial factor in improving the performance of photocatalysts. The electric field
462 inside the substance induces a static force on the charges in the opposite direction,
463 which makes it possible to increase their lifetime by limiting their recombination
464 [101]. This electric field also promotes their transport to the interfaces where the
465 chemical reactions of interest occur (**Fig. 8**). Discussions regarding the potential role
466 of persistent polarizations in facilitating efficient separation of electrons (e^-) and holes
467 (h^+) have started to appear in the literature [150–152].

468 However, it is essential to note that in the case of imogolite, the nanotube
469 serves a unique dual role, acting as both a polar material and a photocatalyst,
470 distinguishing it from the scenario presented here [53,65,100,119]. The inherent
471 polarization of imogolite nanotubes, coupled with their photocatalytic activity, creates
472 a synergetic effect that significantly enhances their performance in light-driven
473 catalytic reactions. This dual functionality showcases how imogolite seamlessly
474 integrates both the roles of a polar medium and a photocatalyst, offering a unique
475 and promising platform for efficient photoinduced catalysis, where the material's
476 polar nature finely tunes charge separation and transport.

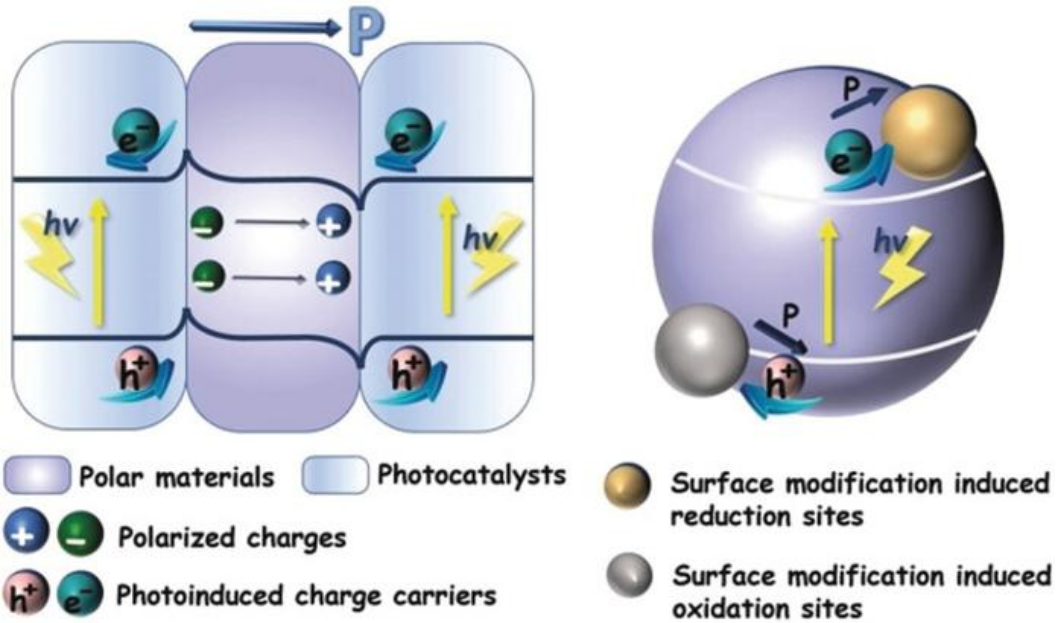

Fig. 8. The scheme for polarization promoted surface charge separation. Reproduced with permission from [101] .Copyright (2019), Wiley.

In this context, Gustafsson and co-workers first discussed the intrinsic polarization in natural imogolite in 2001 [153]. They explained that the pKa of the hydroxyl functions that compose the inner and outer surfaces could not justify the evolution of the charge of the outer surface of INTs as a function of pH. In general, in aluminum oxides, the aluminol functions, similar to imogolite, remain uncharged over a broad pH range, from 0 to 11.9 [153]. Moreover, surface complexation of ions by these groups is not considered possible. Consequently, they assumed that the outer tube walls are unreactive toward ions. The authors, therefore, proposed a model in which negative and positive charges accumulate on the internal and external surfaces of the nanotube, respectively. These charges are not dependent on the pH. They thus defended the existence of polarization through the wall.

Teobaldi's group conducted density functional theory (DFT) calculations concerning INTs, focusing on various physico-chemical structures [57,154]. These simulations have shown that INTs exhibit a persistent polarization corresponding to a

spatial separation of the VB and CB in real space (**Fig. 9**) [57,154]. This separation enhances the separation of holes (h^+) and electrons (e^-) through optical charge-transfer excitations inside the walls of the nanotubes.

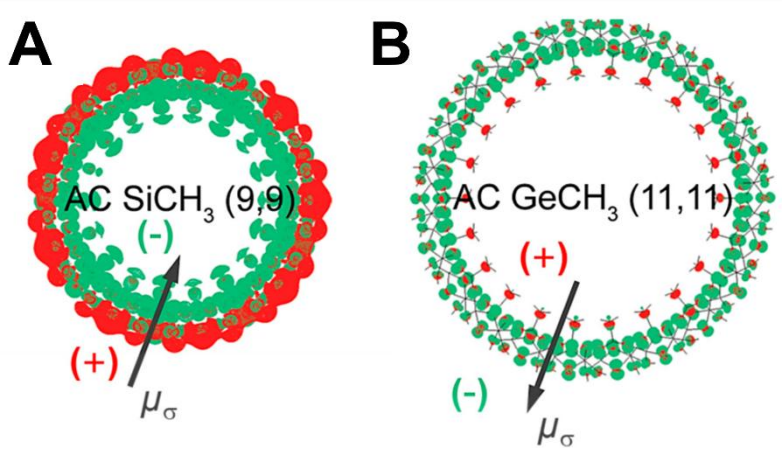

Fig. 9. Front image of armchair methylated INTs $(OH)_3Al_2O_3Y(CH_3)$ showing the real-space separation between the boundaries of the conduction band (red) and valence band (green). Y = Si in (A) and Ge in (B). The direction of the permanent dipole surface density μσ of the nanotube wall is indicated by the black arrow. Reproduced with permission from [122], Copyright (2018) Nature.

Furthermore, the excellent chemical separation characteristics of hybrid hydrophobic/hydrophilic Imo NTs, along with their ease of modification [136,138,155,156] could be very favorable for the effective separation of photo-oxidized and photo-reduced reactants and products (**Fig. 10A** and **Fig. 10B**). Articles discussing the potential beneficial impact of permanent polarizations on the effective separation of holes (h^+) and electrons (e^-) have started to appear in the literature [65,100,154,157], prompting increasing interest in this field.

Although INTs have been utilized as catalyst supports (as discussed in section 4) and initial findings have been reported regarding their efficacy in the photocatalytic decomposition of organic dyes [40,97,98], this subject is yet to be explored.

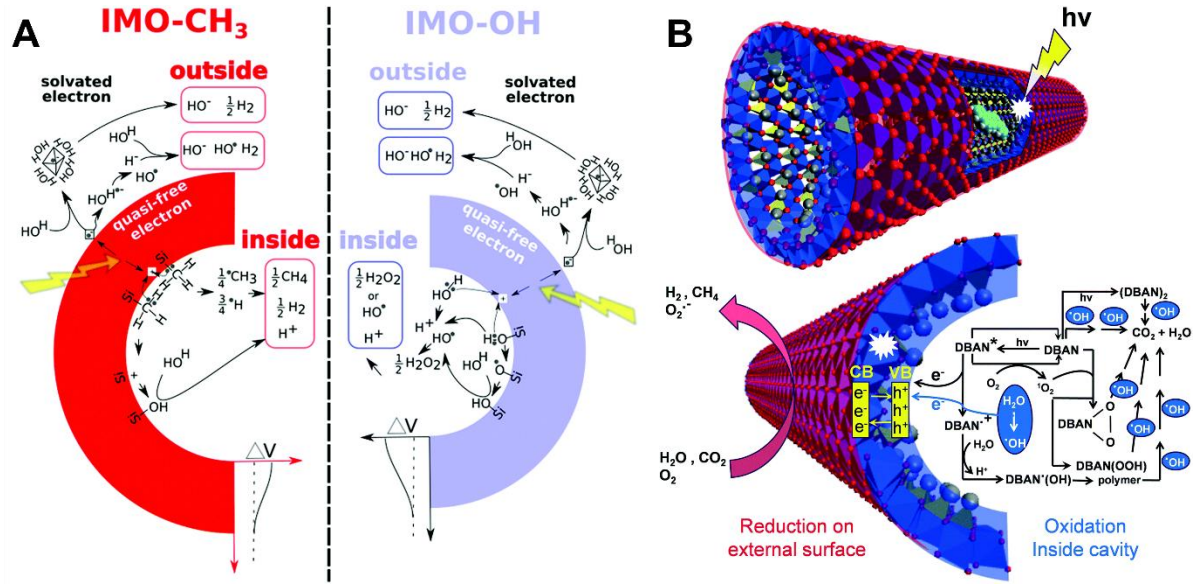

Fig. 10. **A**) Schematic of the reaction mechanisms at play in two types of imogolites (IMO-CH_3 and IMO-OH). For clarity, water radiolysis was left out. The intra-wall electric field (ΔV), which drives charge separation, is schematically represented. Reproduced with permission from [66], Copyright (2021) The Royal Society of Chemistry. **B**) Illustration of potential key photodegradation pathways for DBAN enclosed in Imo-CH_3 nanotubes in an aqueous medium. Reproduced with permission from [96], Copyright (2021) The Royal Society of Chemistry.

3.3. Structural and physiochemical properties of chrysotile

Chrysolite is a hydrated magnesium silicate with a stoichiometric composition of $Mg_3Si_2O_5(OH)_4$. Natural chrysotile, commonly known as white asbestos [158,159], is part of the serpentine group of minerals. It has found extensive applications across diverse industries thanks to its remarkable properties, including high tensile strength, flexibility, and excellent resistance to heat and chemicals. However, despite its extensive use, there are growing concerns about the potential health risks of exposure to chrysotile fibers. Inhalation of these tiny fibers can result in severe respiratory problems, including lung diseases like asbestosis and mesothelioma, which is a rare and aggressive form of cancer [159–161].

Chrysolite consists of a silicate sheet $(Si_2O_5)_n^{2n-}$, where the neighboring tetrahedra share the oxygen atoms present in the tetrahedron, and a non-silicate sheet $[Mg_3O_2(OH)_4]_n^{2n+}$ [162]. The curvature of the sheets spreads along a favored axis, giving rise to the tubular chrysotile structure similar to that seen for halloysite (**Fig. 11A**) . The concentric sheets developing the fibers exhibit a curvature radius ranging from 2.5 to 3.0 nanometers for the inner layers, expanding to approximately 25 nanometers for the outer layers. As a result, unit fibers (fibrils) have external diameters that vary between 20 and 50 nanometers [163]. Researchers have tried to refine chrysotile's structure through the Rietveld method. In a study conducted by Falini et al. [164], they refined nano-chrysotile within the monoclinic Cc space group, determining lattice constants a=5.340(1), b=9.241(1), c=14.689 (2) Å, and β=93.66 (3)° [165]. The chemical composition of chrysotile differs depending on the mineral deposit. In fact, the substitution of silicon and magnesium can occur in chrysotile. In the brucite layer, it is possible to substitute magnesium with Mn^{2+}, Fe^{2+}, or Ni^{2+} [166]. Conversely, in the silicate layer, silicon can be replaced by Al^{3+} or rarely Fe^{3+} [167] (**Fig. 11B**).

Chrysotile exhibits chemical stability, incombustibility, and exceptional thermal insulation properties [168]. Additionally, its fibrils are known for their strength and remarkable flexibility. These fibers exhibit low thermal conductivity (0.3-0.4 W/(m K)), exceptional ability to withstand high temperatures, and a high melting point (approximately 1500 °C). They possess greater rigidity compared to steel, are impressive, resistant to corrosion, and not expensive compared to synthetic fibers [169].

The investigation conducted by Lourenço et al [171]. on the electronic properties of Single-Walled Chrysotile Nanotubes (NTs) using the self-consistent

charge density-functional tight-binding method (SCC-DFTB) sheds light on the intricate electronic structure of chrysotile. Their findings reveal intriguing insights into the total (DOS) and partial density of states (PDOS) of zigzag (40,0) and armchair (25,25) chrysotile NTs (**Fig. 11C**). Surprisingly, they discovered that the chirality and size of the NTs do not significantly alter their electronic structure, as evidenced by the similarity in DOS and PDOS profiles (Figure 5). Specifically, in the valence band, the predominant states are attributed to oxygen atoms, while in the conduction band, electronic states of silicon atoms play a pivotal role in shaping the total DOS. Interestingly, the contribution of magnesium and hydrogen atoms to the total DOS is comparatively smaller than that of silicon and oxygen in both valence and conduction bands.

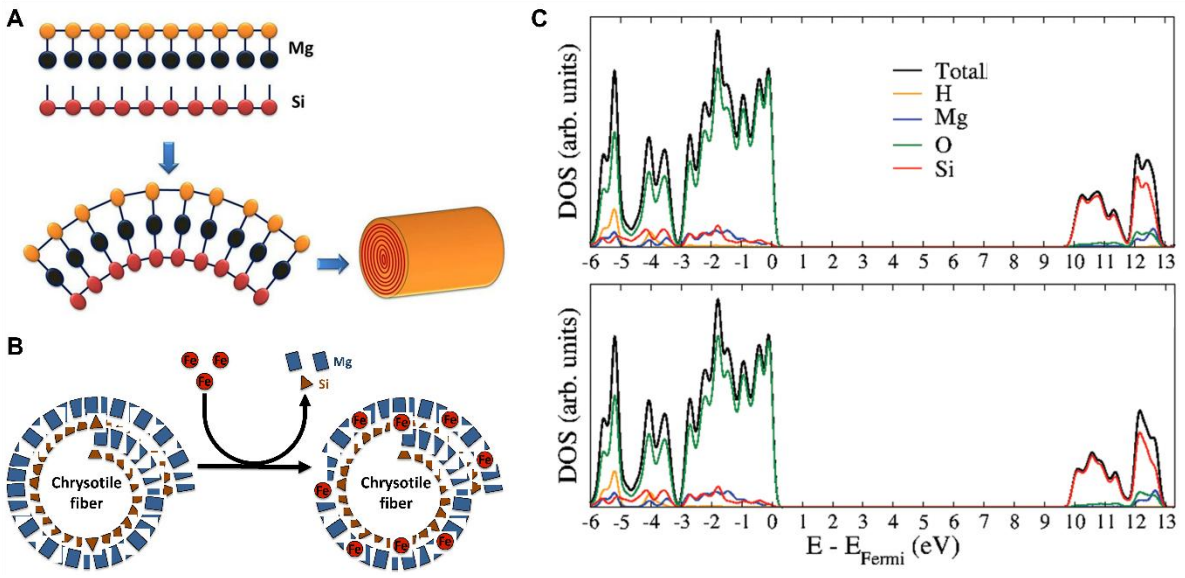

Fig. 11. **A**) structure of chrysotile. Reproduced with permission from [170], Copyright (2013) Scientific research. **B**) Depiction of magnesium and silicon substitution by iron in the chrysotile fiber structure. Reproduced with permission from [167], Copyright (2020) MDPI. **C**) Total and partial density of states (PDOS) of the (a) zigzag (40,0) and (b) armchair (25,25) chrysotile nanotubes. Reproduced with permission from [171], Copyright (2012), American Chemical Society.

An electron-microscopic study of chrysolite by Voitylov et al. showed diverse morphologies of nanotubes: cones, cylinders, and socket tubes (**Fig. 12**).). Conical nanotubes exhibit external diameters between 20 and 50 nm, while cylindrical nanotubes have external diameters between 20 and 70 nm. The inner diameter of cylindrical nanotubes is 35 nm. Notably, various other forms of chrysotile can also be found in nature (e.g., cylinder-in-cylinder, tube twins, rectilinear cylinders, cone-in-cone tubes, and cylinders with cup-like ends) [169]. It was revealed that synthesis conditions, including factors like temperature, hydrothermal treatment duration, and the composition of the precursor solution, influence specific morphological characteristics of the nanotubes [172].

Chrysotile has attracted significant attention due to its catalytic activity. The abundance of active sites and its high surface area make chrysotile-based catalysts highly promising for various chemical reactions [173]. These catalysts have demonstrated remarkable efficiency in numerous processes, such as polymerization, hydrolysis, reduction, and oxidation [174–177], making them versatile tools for organic synthesis and industrial applications. The distinctive fibrous morphology of chrysotile nanotubes creates an environment conducive to catalytic reactions, leading to improved selectivity and reaction kinetics.

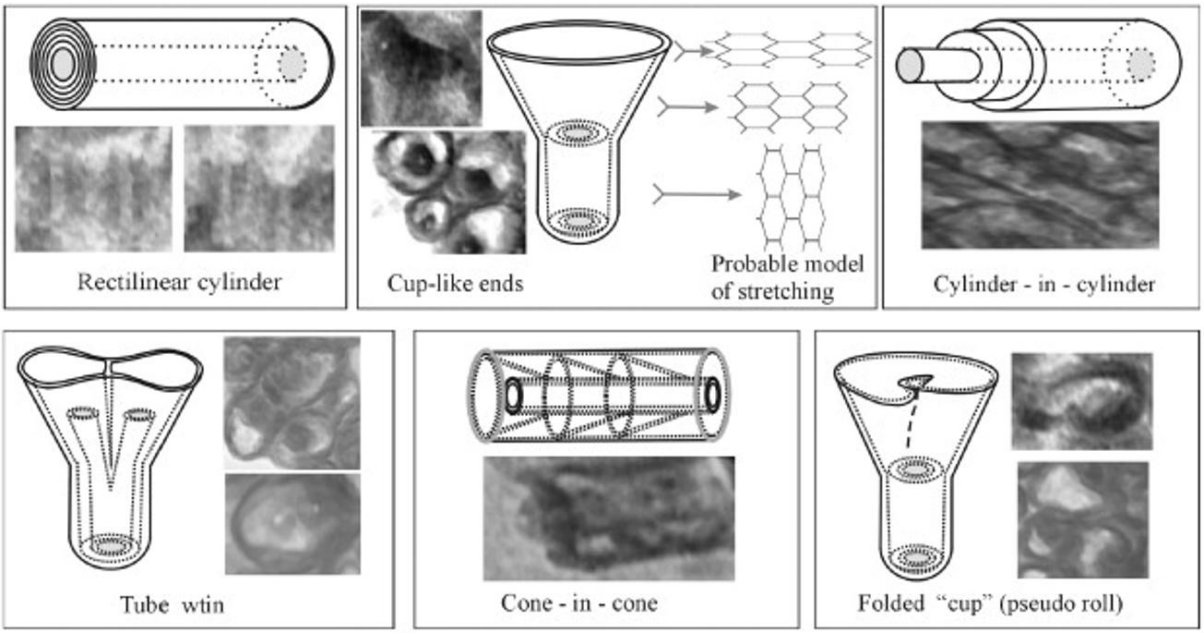

Fig. 12. The hypothetical models of the chrysotile nanotubes. Reproduced with permission from [169], Copyright (2011) Elsevier.

4. Applications in photocatalysis

In the realm of phototcatalysis, the interface interaction between tubular clay carriers and active components emerges as a pivotal determinant of performance and efficacy. Photocatalysis relies on the intricate interplay between light-absorbing materials and catalytic species to drive chemical transformations for environmental remediation and energy conversion [178,179]. Within this context, the interface interaction orchestrates the spatial arrangement, charge transfer dynamics, and surface chemistry crucial for photogenerated charge carrier migration and surface redox reactions [178–180]. Physical adsorption of photocatalytic species onto the tubular clay surfaces establishes localized reaction sites, amplifying photon capture efficiency and catalytic activity [180–184]. Chemical bonding between the active components and the clay matrices bolsters stability, mitigates photocorrosion, and prolongs catalyst lifespan under harsh irradiation conditions. Electrostatic

interactions, in turn, regulate the distribution and orientation of photoactive species, optimizing interfacial charge transfer processes and redox kinetics [180–185]. Surface coordination phenomena further fine-tune the electronic structure and surface reactivity of the catalyst, tailoring its performance to specific phototcatalytic applications [181–185].

Due to clay's excellent structural properties and surface areas, nanotubes (chrysotile, halloysite, and imogolite) can be used as a catalyst or co-catalyst in photocatalytic systems. This section summarizes the application of clay nanotubes in photocatalysis from four aspects: Pollutant degradation in the water and air, photocatalytic hydrogen evolution reactions, disinfection of bacteria, and photocatalytic nitrogen fixation.

4.1. Degradation of organic pollutants by photocatalysis

With the development of modern industry, a wide range of toxic pollutants, including synthetic dyes, phenol, and pharmaceutical substances, have been discharged into the air, water, and soil, resulting in substantial harm to the environment and living organisms. Thus, various approaches, including chemical degradation, physical adsorption, and biodegradation methods, have been employed for environmental restoration [186–193]. However, many traditional approaches to environmental remediation were deemed ineffective and had the potential to result in secondary pollution. In recent years, solar-driven photocatalysis technology has emerged as an environmentally friendly, efficient, and cost-effective solution for addressing environmental pollution removal. Due to their excellent structural properties and surface areas, clay nanotubes have been attractive candidates for utilizing eco-friendly waste treatment in air and water environments.

For instance, Katsumata et al [67]. successfully crafted a nanotubular imogolite structure through a hydrothermal process, subsequently employing it to fabricate composites of imogolite/TiO_2 and imogolite/Cu(II)-grafted TiO_2 (**Fig, 13A)**. The authors reported that, under visible light illumination, the composite imogolite/Cu(II)-grafted TiO_2 demonstrated a notable improvement in its efficiency for the photodegradation of acetaldehyde when compared to both TiO_2 and Cu(II)-grafted TiO_2. Furthermore, this enhanced activity appeared less influenced by the relative humidity. This result suggests a unique role of imogolite in effectively adsorbing acetaldehyde. The researchers found that imogolite adsorbs acetaldehyde and captures intermediates, including CH_3COOH, during the acetaldehyde decomposition process. These intermediates are subsequently degraded to CO_2 through the action of radical species generated on the catalyst surface. The authors suggested the imogolite-containing composite as a highly efficient photocatalyst and could utterly eliminate the VOCs [67].

Similarly, Liu et al. [45] created a novel chrysotile@ZnO nanocomposite by coating ZnO on the surface of chrysotile, as illustrated in (**Fig 13B**). The photocatalytic performance of the chrysotile@ZnO nanocomposite was evaluated under UV light irradiation (365 nm), focusing on its capability for the photocatalytic decomposition of methylene blue (MB) dye. It has been stated that ZnO nanoparticles are homogeneously distributed across the chrysotile surface (**Fig, 13C**). The team achieved up to 99.5% MB dye degradation after 60 min illumination compared with only 76% obtained with the ZnO, showing that the composite displayed improved light absorption and charge transport. Furthermore, it showcased a capacity for efficient recycling, retaining effectiveness even during the third cycle. The bandgap and photon-hole recombination rate of ZnO nanoparticles are lowered

by the combined effects of surface passivation and chrysotile's interfacial action. This improvement results in enhanced photodegradation of organic pollutants, introducing a new level of performance to chrysotile (**Fig, 13D)**.

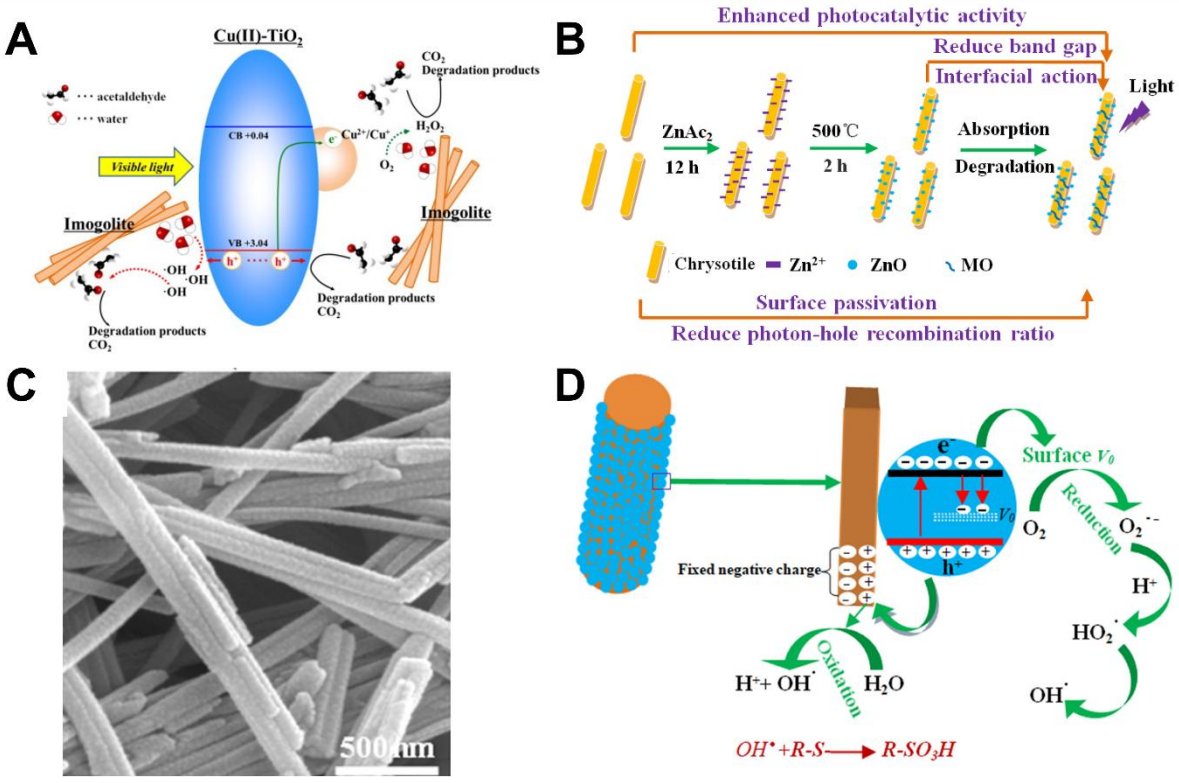

Fig. 13. **A)** Cu(II)-grafted TiO_2-imogolite composite: Potential photodegradation mechanisms of acetaldehyde under visible light irradiation. Reproduced with permission from [67]. Copyright (2013) Elsevier. **B)**. Graph illustrating the chrysotile@ZnO nanocomposites' formation process. **C**) SEM images of chrysotile@ZnO nanocomposites. **D**) Diagrammatic representation of MB's photocatalytic degradation process over chrysotile@ZnO nanocomposites in the presence of UV light. Reproduced with permission from [45], Copyright (2020) Elsevier.

In a captivating study conducted by Wu and his colleagues [194], they explored the potential of novel hetero-structural g-C_3N_4/TiO_2/commercial halloysite composites in the elimination of ciprofloxacin from wastewater (**Fig, 14A)**. Their findings reveal that the introduction of halloysite nanotubes (HNTs) and the g-C_3N_4-TiO_2 heterojunction significantly augmented the efficiency of charge transfer and

separation among photogenerated electron-hole pairs. This enhancement endowed the g-C_3N_4/TiO_2/HNTs hybrid material with remarkable photoelectric performance and stability. Notably, the composite achieved an impressive 87% degradation of ciprofloxacin within 60 minutes, owing its rapid photoelectron-hole pair transfer and separation capabilities. The most significant result was the remarkable reusability of the C_3N_4/TiO_2/HNTs nanocomposites even after 4 cycles.

In a related investigation, Li et al. [195] investigated the photocatalytic degradation of chlortetracycline, a common antibiotic, under visible light irradiation. They achieved this by immobilizing $LaFeO_3$, one of the most important perovskite-type semiconductor, onto the surface of halloysite nanotubes (HNTs) through a simple sol-gel method (**Fig, 14B)**. Thier findings indicated that untreated halloysite lacked photocatalytic activity. However, when chlortetracycline was exposed to pure $LaFeO_3$, 74% of the drug degraded within a 90 min. Notably, the degradation rate increased to 87% with the use of $LaFeO_3$/HNTs as catalyst, underscoring the enhanced performance facilitated by this composite. The improved efficacy was attributed to the adsorptive capacity of HNTs and the augmented electron transfer capacity of $LaFeO_3$, providing insights into the synergistic mechanisms underlying the composite's photocatalytic behavior.

In the other study, Mishra et al [99]. developed a TiO_2@HNT photocatalyst through a combination of sol-gel and phase inversion methods, yielding a stable and highly efficient photocatalyst (**Fig, 14C)**. This composite exhibited enhanced photocatalytic activity attributed to the electrostatic interaction between TiO_2 and the HNT surface. Under UV light, the nanocomposite effectively degraded 87.47% and 96.87% of methylene blue and rhodamine B, respectively. The strong electrostatic interaction between TiO_2 and HNTs facilitated the generation of more electron-hole

pairs, thereby increasing photocatalytic activity. Particularly for methylene blue and rhodamine B dyes, which carry positive charges, HNTs improved the stability and supply of photo-generated charges, enhancing dye molecule absorption on the photocatalyst. This effect stemmed from electrostatic attractive and repulsive forces originating from the negatively charged HNTs surface. Crucially, the TiO_2@HNTs photocatalyst demonstrated non-photo-corrosive behavior during three consecutive cycles of photocatalytic degradation, highlighting its suitability for practical applications.

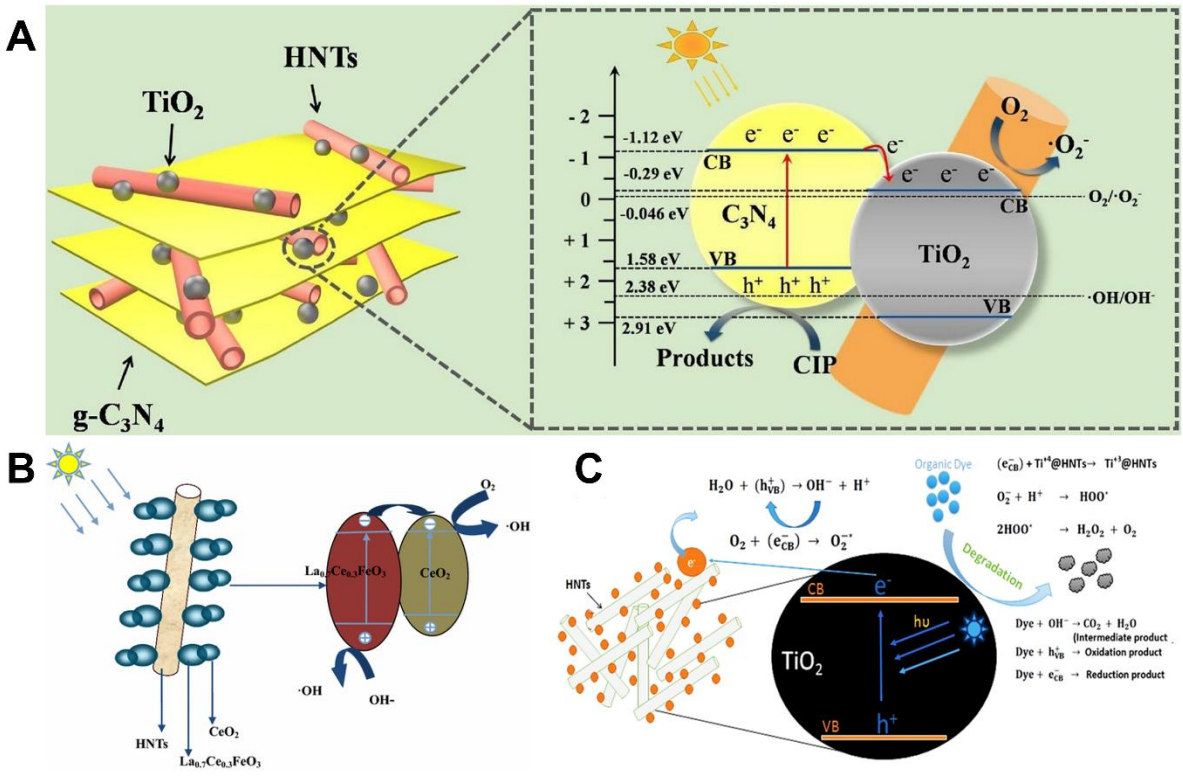

Fig. 14. **A)** Schematic of possible mechanism for photodegradation of CIP over g-C3N4/TiO2/HNTs heterojunction composites. Reproduced with permission from [194]. Copyright (2018) Elsevier. **B)**. Schematic illustration of photocatalysis mechanism for $La_{0.7}Ce_{0.3}FeO_3$/HNTs. Reproduced with permission from [195]. Copyright (2016) springer. **C)**. Schematic representation of the photocatalytic activity of TiO_2@HNTs photocatalyst. Reproduced with permission from [99]. Copyright (2019) springer.

Jatav et al. [196] recently conducted a hydrothermal growth of In_2S_3 on aluminogermanate double-walled imogolite nanotubes. Their investigation involved using methyl orange (MO) as the target pollutant for assessing photocatalytic performance. The findings demonstrated that the presence of INT facilitated the growth of In_2S_3 on its surface, while the morphology of In_2S_3 was significantly affected by the reaction time. When the reaction time extended to three and five hours, the tubular morphology of INT transformed into elongated sheets. Remarkably, the photocatalytic study revealed that the In_2S_3-decorated INT showed an improvement in the rate of MO photocatalytic degradation of about 400% when compared to pristine In_2S_3, despite the composite showing a 14% increase in bandgap. This improvement in photocatalytic performance was ascribed to the exceptional mobility of photogenerated holes, which sped up MO's oxidative processes directly.

A literature survey reveals that using tubular clay minerals increases the photocatalytic activity of several photocatalyst materials [47,197–200]. Among these tubular clay materials, Halloysite stands out as one of the most widely used for photocatalytic applications. Due to its tubular structure and large specific surface area, it is used as a stabilizer to inhibit nanoparticle aggregation. Christoforidis et al. [200] exploited the self-assembly method to generate a hetero-architecture of Halloysite-graphitic carbon nitride (gC_3N_4) with different mass ratios 2, 4, 6, and 10 wt.% of Halloysite (denoted by CNH-x). Utilizing both pure visible light and solar light simulation, the composites were then tested for the photodegradation of neutral, positively, and negatively charged pollutants, including methyl orange (MO), phenol, and MB. TEM images (**Fig, 15A)** proved that the deposition of small-sized g-C_3N_4 sheets onto the halloysite surface showed no apparent aggregation. It has been

751 experimentally provided that various compositions of Hall@gC_3N_4 composites
752 exhibited photocatalytic activities greater than bare Halloysite and gC_3N_4. The best
753 composite, CNH-2 catalyst (the one containing 4 wt% of HNTs), was able to degrade
754 MB dye within 4h under solar light (**Fig, 15B**). Moreover, after four cycles of MB
755 degradation under solar-like light irradiation, the CNH-2 composite displayed no
756 noticeable decline in photocatalytic activity, signifying its remarkable photostability.
757 Moreover, adding HNTs into gC_3N_4 led to an improvement in photocatalytic activity
758 compared to gC_3N_4 alone for the degradation of neutral and positively charged
759 pollutants. This enhancement was attributed to the electrostatic interaction between
760 the negatively charged Halloysite surface and the photogenerated e^-/h^+ in gC_3N_4,
761 which reduced charge carrier recombination rate (**Fig, 15C)**. The negatively charged
762 surface of Hal served two purposes in the case of the positively charged pollutant,
763 such as MB: it enhanced MB adsorption and moved it close to graphitic carbon
764 nitride. Conversely, the photocatalytic degradation of the negatively charged
765 substrate, like MO, was similar to that of g-C_3N_4. In this case, while the repulsion
766 between the negatively charged Halloysite and the negatively charged substrate
767 (MO) had an adverse impact, it actually led to improved charge separation,
768 consequently boosting the overall activity. Overall, Halloysite nanotubes (HNTs) had
769 demonstrated to have a double function: (a) improving the abundance and stability of
770 the photogenerated charges; (b) enhancing the adsorption of MB dye on the
771 nanocomposite. These two functions are induced by electrostatic forces, combining
772 attraction and repulsion, stemming from the negatively charged surface of HNTs.

773 Likewise, the negatively charged halloysite nanotube surface combined with
774 the electrostatic interactions of Ag cations served as a starting point to synthesize a
775 core-shell structured photocatalyst based on halloysite [199]. Subsequently, the

nucleation and growth of Ag_3PO_4 led to the formation of Ag_3PO_4@halloysite nanotubes (Ag_3PO_4@HNTs) nanocomposite (**Fig, 15D**). The nanocomposites exhibited remarkable photocatalytic effectiveness in decomposing RhB dye under ultraviolet illumination. The outstanding photocatalytic capabilities of these photocatalysts were attributed to both halloysite and Ag_3PO_4; mainly, halloysite shells' presence guarantees rapid dye adsorption onto the catalyst surface and concurrently reduces the band gap of Ag_3PO_4, as well as minimizing the recombination rate. The decrease in recombination was attributed to the lowered interface defect density and the field-effect passivation produced by the negative fixed charge within the halloysite shell.

Many works have been conducted on the photocatalytic activities of clays nanotube photocatalysts to remove different types of organic pollutants, as summarised in Table 1.

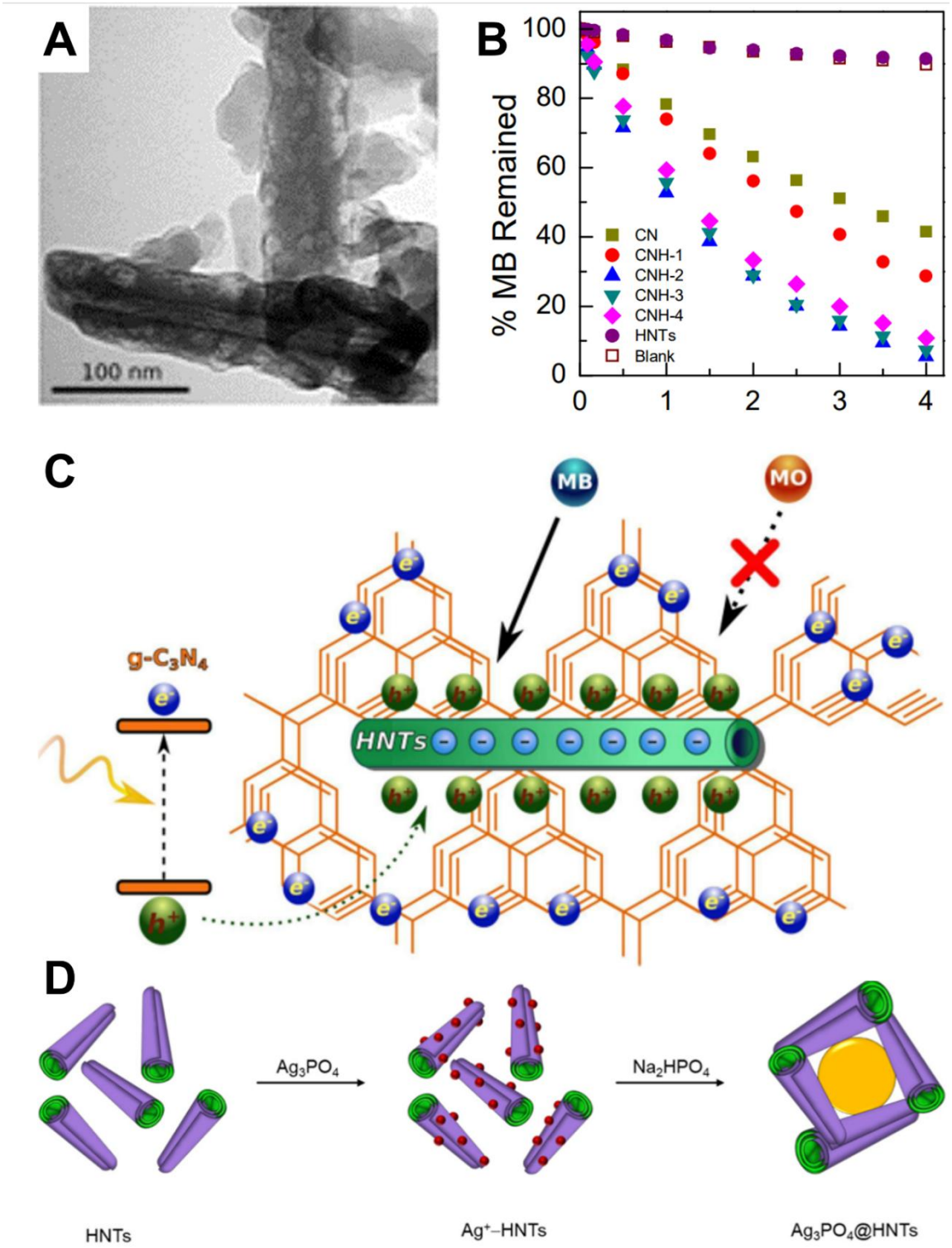

Fig. 15. **A)** TEM images of Halloysite nanotubes@g-C_3N_4, **B)** Photocatalytic degradation of MB dye over Halloysite nanotubes@g-C_3N_4 under solar light irradiation. **C)** Proposed mechanism of the enhanced charge carries separation in the Halloysite nanotubes@g-C_3N_4 nanocomposites. Reproduced with permission from [200], Copyright (2016) Royal Society of Chemistry. **D)** Schematic Illustration of core-shell structured Ag_3PO_4@Hal nanocomposites formation process Ag_3PO_4@Hal nanocomposites. Reproduced with permission from [199], Copyright (2017) Elsevier.

798 **Table. 1**. Studies of clay nanotubes photocatalysts for various pollutants
799 degradations

Clay nanotube	Photocatalyst	light source	Pollutants	Photocatalytic degradation activity	Ref
Chrysotile	Chrysotile@SnO_2	Hg lamp (centered at 450 nm, 250 W)	MB dye	99% (90 min)	[47]
	Chrysotile@ZnO	250 W high-voltage Hg lamp (365 nm)	MB dye	99.5% (60 min)	[45]
	Chrysotile@ZnO	365 nm UV light	4-nitrophenol	39% (300 min)	[98]
	Chrysotile@TiO_2	Xe light source	CV dye	~66% (240 min)	[201]
Imogolite	Fe-0.050-MeIMO	8 W mercury vapor lamp emitting at 254 nm	TRZ dye	100% (300min)	[202]
	Me-IMO	8 W mercury vapor lamp emitting at 254 nm	TRZ dye	80% (300min)	[202]
	INT-In_2S_3	300 W Xe lamp	MO dye	90% (120min)	[196]
	TiO2-IMO	UV light lamp (1.0 mW/cm2)	CH3CH2	90% (60min)	[67]
Halloysite	Halloysite@Fe_2O_3	UV low pressure Hg immersion lamp TNN 15/32	2,6-dichloroaniline (26DCA)	84.6% (300 min)	[203]
	Halloysite@TiO_2	UV low pressure Hg immersion lamp TNN 15/32	2-chloroaniline (2CA)	84.9% (300 min)	[203]
	Ag_3PO_4-25 wt% HNTs	26 W Sylvania visible lamp.	naproxen sodium	~80% (10 min)	[204]
	La_2O_3/$CeVO_4$@halloysite	300 W Xenon lamp (λ ≥ 420 nm)	TC dye	87.1% (60 min)	[205]
	N-TiO_2/ Halloysite	xenon lamp, PLS-SXE300, 300W	phenol	70% (150 min)	[206]
	Ag_2CO_3-75 wt.% Halloysite	26 W Sylvania visible lamp	RhB dye	97 % (40 min)	[207]
	CdS@Halloysite	xenon lamp, 500W	TC dye	93% (60 min)	[208]
	Ag@ Halloysite	500 W mercury lamp	TC dye	95.81% (80 min)	[209]
	Ag/AgBr/ Halloysite	200 W xenon lamp with a UV cutoff filter	RhB dye	98%% (30 min)	[210]
	AgNPs@N-Halloysite	500 W xenon lamp	MB dye	90% (60 min)	[211]
	Co_3O_4@ Halloysite	60 W high-pressure mercury lamp	MB dye	97 % (120 min)	[197]
	Halloysite@W18O49	300 W Mercury lamp	MO dye	99 % (120 min)	[198]
	Bi^{3+}- CdS/Halloysite	500 W xenon lamp	TC dye	90% (30 min)	[212]
	Ce-TiO_2/HNT	300 W Xe lamp (λ > 420)	Tetracycline	78% (60 min)	[213]
	Carbon-TiO_2-HNT (8%)	50 W UV lamps (λ < 420 nm)	MB dye	81% (90 min)	[214]
	Pani-TiO_2-HNT (0.5 g/L)	XPA-7 photochemical system (800 W Xe lamp)	RhB dye	76.49 % (360 min)	[215]
	Amylose-HNT-TiO_2	12 W UV lamp (λ = 253 nm)	4-nitrophenol	90% (240 min)	[216]

800

4.2. Photocatalytic water splitting

Photocatalytic water splitting has been widely explored as a vital clean energy source. Photogenerated electrons and holes are simultaneously generated when exposed to light in the general mechanism of photocatalytic water splitting for hydrogen production. Following this, electrons and holes migrate to the photocatalyst's surface to participate in the reaction. The photocatalyst's potential and valence band level should be positioned at a lower energy level than H^+/H_2 and higher than OH^-/O_2 potential [9,15,217]. To ensure a successful H_2 evolution reaction, the photocatalyst's conduction band (CB) energy level must be below 0 V versus the normal hydrogen electrode (NHE) at pH 7. Similarly, for effective H_2O oxidation, the valence band (VB) energy level should be above 1.23 V versus NHE. Therefore, theoretically, for water splitting, the lowest bandgap is 1.23 eV. These energy level requirements are vital to promote favorable redox processes during photocatalysis. Recently, it was proven that using clay nanotubes could improve photocatalytic activity and facilitate separation and recycling [205,208]. Hojamberdiev and co-workers [218] stated that the synthesis of a novel $Ni(OH)_2$@g-C_3N_4/halloysite composite photocatalyst by mixing an easily prepared gC_3N_4 with low-cost $Ni(OH)_2$ nanoplatelets, inexpensive and earth-abundant halloysite nanotubes. The obtained composite was used as an efficient photocatalyst for hydrogen evolution. As-prepared photocatalysts' hydrogen evolution reaction activity was assessed using an aqueous solution with 10 vol% methanol as a sacrificial agent. The investigation of the $Ni(OH)_2$ loading effect showed that the 1 wt% $Ni(OH)_2$@g-C_3N_4/halloysite photocatalyst exhibited the maximum photocatalytic hydrogen evolution rate (18.42 $\mu mol \cdot h^{-1}$) compared to $Ni(OH)_2$@g-C_3N_4 (9.12 $\mu mol \cdot h^{-1}$) and was 40 times higher than g-C_3N_4 alone (0.43 $\mu mol\ h^{-1}$) (**Fig. 16A**). Furthermore, 1 wt% $Ni(OH)_2$@g-C_3N_4/halloysite photocatalyst showed negligible

decrease in H_2 evolution activity after three cycles (**Fig. 16B**). The halloysite's negatively charged surface, which effectively traps photogenerated holes, lowers the rate of electron-hole recombination, and lengthens the electron lifespan, provided an explanation for these results (**Fig. 16C**). Moreover, a computational model was employed to assess the adsorption properties of H_2O and MeOH molecules on the catalyst surface. The findings indicated that the presence of halloysite, g-C_3N_4 and $Ni(OH)_2$ enhanced the adsorption of water and methanol on the co-catalyst surface.

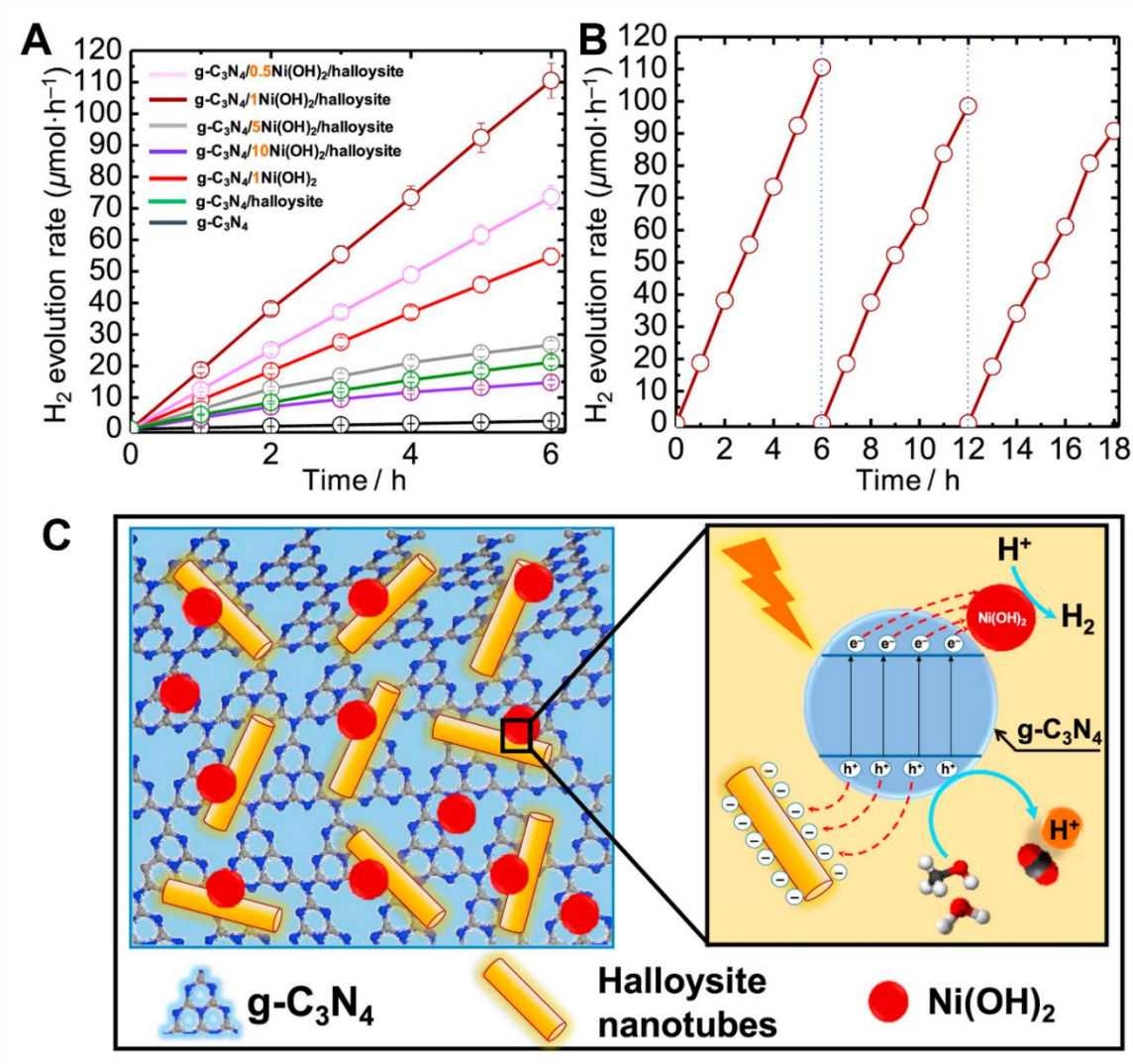

Fig. 16. **A)** $Ni(OH)_2$@g-C_3N_4/halloysite nanocomposites: reaction time courses of visible light-driven hydrogen evolution. **B**) Reaction time courses of visible-light-driven hydrogen evolution on 1.0$Ni(OH)_2$@g-C_3N_4/halloysite nanocomposite for three successive runs. **C**) Graphical representation of the evolution of photocatalytic hydrogen evolution over developed nanocomposites, showing the separation and

transfer of photogenerated charge carriers. Reproduced with permission from [218], Copyright (2019) Elsevier.

Recently, Lu et al. [219] successfully synthesized several $K_{0.5}Na_{0.5}NbO_3$/halloysite nanocomposites by changing the halloysite concentration from 0 to 25 wt.% via a solid phase reaction process. These hybrid samples were then used to analyze the photocatalytic hydrogen evolution performance under UV light illumination (Xenon arc lamp). The authors demonstrated that by incorporating halloysite (HNTs), the absorption spectrum of $K_{0.5}Na_{0.5}NbO_3$ (KNN) exhibited a substantial enhancement in the UV region, with the absorption intensity in the 200-300 nm range increasing approximately two-fold (**Fig. 17A**). Introducing HNTs into KNN reduced the band gaps from 3.03 eV to 2.64 eV (**Fig. 17B**). Moreover, the authors demonstrated that the conduction band (E_{CB}) of KNN-5wt%HNTs nanocomposite was changed to a lesser value from -1.13 eV to -1.18 eV compared with the pure $K_{0.5}Na_{0.5}NbO_3$, providing more straightforward water reduction to hydrogen. Notably, the composite material KNN-5wt%HNTs demonstrated an excellent hydrogen production performance (31.28 $\mu mol \cdot g^{-1}$ h^{-1}) under UV light irradiation, producing 4.48 times as much H_2 as $K_{0.5}Na_{0.5}NbO_3$. (**Fig. 17C**). The findings of this study confirm that the judicious incorporation of halloysite can improve H_2 production efficiency.

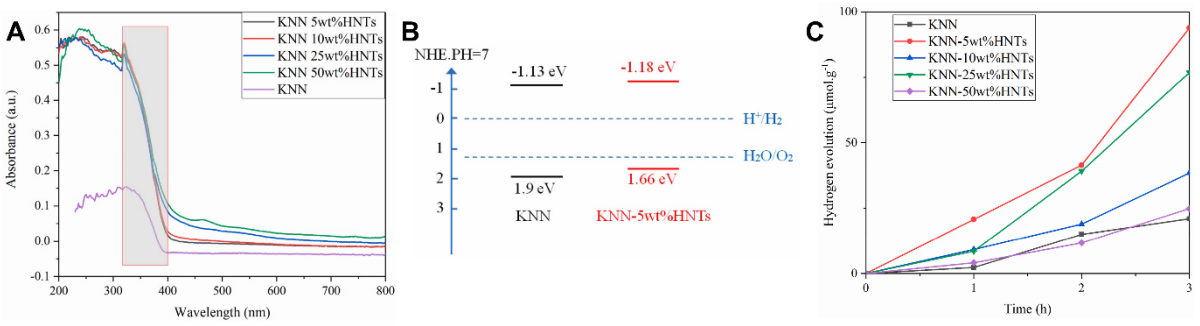

Fig. 17. $K_{0.5}Na_{0.5}NbO_3$-halloysite nanotubes composites. **A)** Spectra of optical absorption, **B**) illustrative sketch of the energy band structures and **C**) hydrogen

evolution reaction for different composites. Reproduced with permission from [219], Copyright (2022) Elsevier.

In a recent research conducted by our research group [220], we achieved a milestone in literature by modifying double-walled aluminogermanate INTs through the incorporation of titanium into the NT walls. The precursor ratio, denoted as x = [Ti]/([Ge]+[Ti]), was varied between 0 and 1. The optical properties of the catalysts we prepared revealed a significant reduction in the band gap (Eg) energy from 4.35 eV (for pristine Ge-DWINT) to 3.96 eV (x = 0.2) and further to 3.92 eV (x = 0.4). Increasing the Ti/Ge ratio consistently decreased the Eg to 3.85 eV. Additionally, Ti-doping initially caused a downward shift of the VB edge (0.13 and 0.43 eV for ratios of 0.2 and 0.4, respectively), followed by an upward shift with further increases in the Ti/Ge ratio. A similar trend was observed for the CB edge, which shifted down to -0.13 eV (for a ratio of 0.4) and up to -1.43 eV (**Fig. 18A**). Interestingly, this evolution, with an optimum around x = 0.4, coincided with the disappearance of nanotubes in favor of boehmite and anatase phases. We examined the photocatalytic properties of the prepared photocatalysts for H_2 production under artificial solar-light irradiation to assess the impact of Ti-doping. Optimal ratios were determined at x = 0.2 and x = 0.4, yielding H_2 production rates of 1509 and 1472 µmol g^{-1}, respectively (**Fig. 18B**). These rates surpassed those of the composites, bare reference, and TiO_2 P25 benchmark NP SC. The enhanced photoactivity stemmed from the narrowed band gap and downward shifts of the CB edges in both composites. As illustrated in **Fig. 18C**, photogenerated charges (e^-/h^+) trigger dissociative adsorption of sacrificial electron donors (SED) and hole scavenging, leading to the release of hydrogen ions (H^+) within the nanotube's internal cavity. Reduction, resulting in H_2 formation, predominantly occurs on the outer surface of the nanotubes, while oxidation predominantly occurs within the nanotubes.

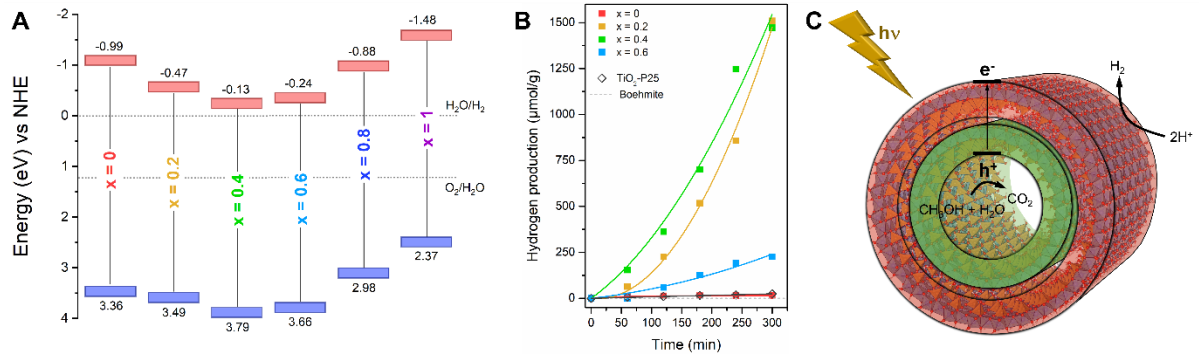

890

891 **Fig. 18**. **A)** energy diagram scheme of the Ti/Ge samples as a function of the
892 substitution ratio. **B)** Hydrogen evolution reaction under solar-light irradiation for a)
893 Ge-DWINT and Ti/Ge samples with different ratios. **C)** Schematic illustration of the
894 proposed H_2 production mechanism. Reproduced with permission from [220],
895 Copyright (2023) wiley.

896

897 In an intriguing study conducted by Zhang et al. [221], they fabricated a
898 satellite-core structured $Cd_{0.5}Zn_{0.5}S$@halloysite hollow nanotubes with a 0D-1D
899 configuration, modified by EDTA with varying amounts, denoted as CZS@HNTs-EX.
900 This was achieved through a facile in-situ assembly approach for photocatalytic H_2
901 evolution. As depicted in **Fig. 19A**, the organic solvent EDTA was initially employed
902 to modify the halloysite, rendering its surface negatively charged. Then, because of
903 the electrostatic attraction Cd^{2+} and Zn^{2+} cations were added and adsorbed onto the
904 halloysite. The addition of thioacetamide finally caused the $Cd_{0.5}Zn_{0.5}S$ nanospheres
905 to grow in situ on the surface of the halloysite that had been modified by EDTA. It
906 was highlighted in this work that the CZS@HNTs-E3% composite exhibited an
907 appealing photocatalytic H_2 evolution after 4 hours of illumination with a yield of
908 102.67 mmol g^{-1} (**Fig. 19B**) and high apparent quantum efficiency (AQE) of 32.29%
909 at λ = 420 nm, higher than majorities of H_2 evolution photocatalysts (**Fig. 19C**). Only
910 a slight decrease in H_2 production was observed after five cycles, while maintaining
911 the crystallinity and morphology of the CZS@HNTs-E3% hollow nanotubes. This
912 highlights the potential of recyclable catalysts for industrial applications.

Furthermore, the authors demonstrated that the enhancement of the photocatalytic of CZS@HNTs-EX was attributed to the succeeding factors: I) the hollow architecture of halloysites caused by several reflections and scattering of light within the cavity, extending the optical transmission path and enhancing the light utilization. II) Halloysites allow an excellent dispersion of $Cd_{0.5}Zn_{0.5}S$, promoting the diffusion of charge carriers to the catalyst-solution interface. III) EDTA embedded on halloysites draws and uses considerable photogenerated h^+, promoting the charge separation of e^- and h^+, permitting more e^- to migrate to the surface of $Cd_{0.5}Zn_{0.5}S$ for participation in the reductive reaction. IV) Owing to the h^+ capture, the h^+-dominated photo-oxidation of S^{2-} in $Cd_{0.5}Zn_{0.5}S$ is hindered, causing excellent photochemical stability in CZS@HNTs-E3.

As far as we are aware, no research has been conducted on the utilization of imogolite or chrysotile for photocatalytic water splitting. It is, therefore, important to pursue efforts in this direction. Given the success of halloysite-based composites in promoting photocatalytic hydrogen evolution, it is reasonable to believe that imogolite and chrysotile might exhibit similar or superior effects.

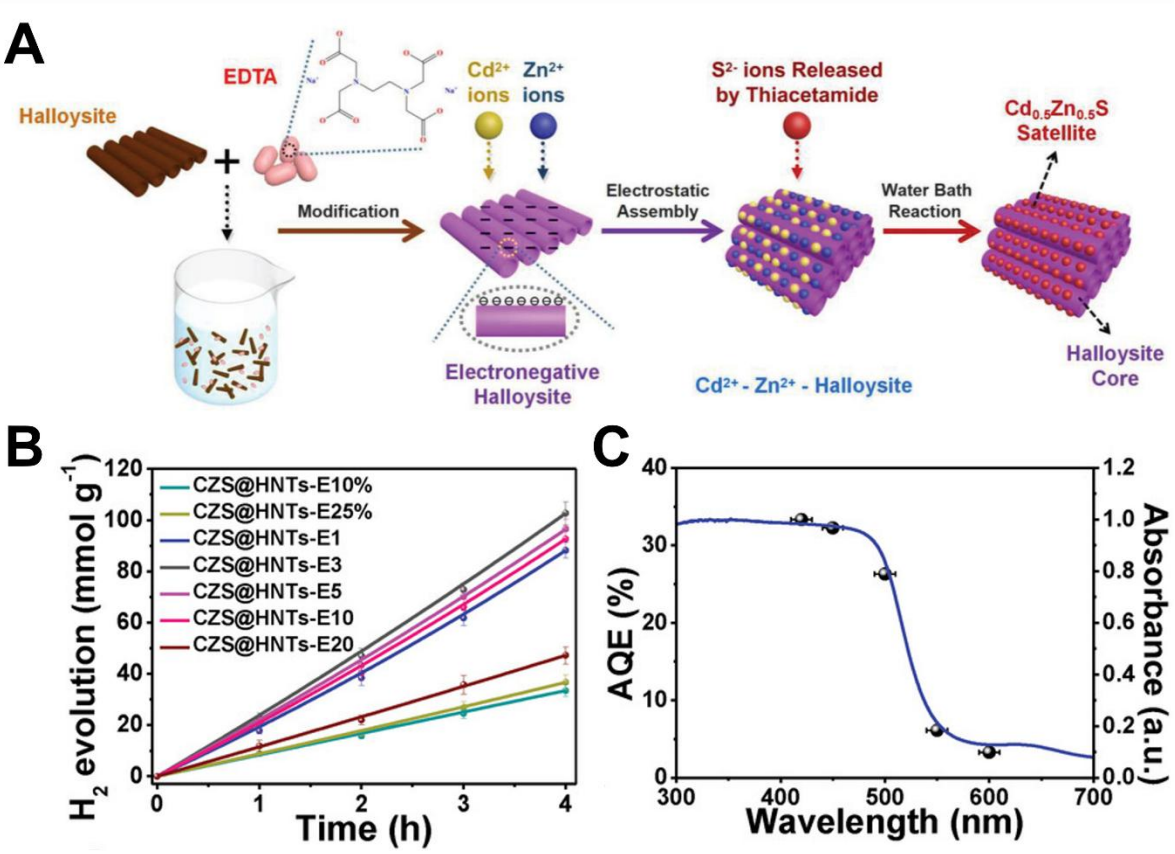

Fig. 19. **A)** Schematic representation of the EDTA-mediated CZS@HNT synthesis process. **B**) Hydrogen evolution time courses for CZS@HNTs-EX samples with varying EDTA to halloysite mass ratios. **C**) Photocatalytic performance of CZS@HNTs-E3 under monochromatic light irradiation: UV–vis spectrum and wavelength dependence. Reproduced with permission from [221], Copyright (2019) WILEY.

4.3. Photocatalytic removal of NOx

Nitric oxide (NOx) emission into the atmosphere is causing increasing concern. This pollutant is produced through fossil fuel utilization and combustion of industrial burners. The NOx emitted into the atmosphere causes acid rain [221–224], climate changes, and ozone layer destruction [222,223]. Thus, its quantitive removal or reduction is highly desired. In fact, numerous catalytic processes for the conversion of nitrogen gases (e.g., NO and NO_2) into oxygen (O_2), nitrogen (N_2), or nitrate (NO_3^-) have been developed, including adsorption, selective catalytic reduction, nonselective catalytic reduction, wet scrubbing, and biofiltration. However, these

947 techniques can only be used to treat NOx in extreme concentrations; their efficiency
948 and economic benefits are reduced at lower NOx concentrations. Currently, for low-
949 concentration NOx in the air at room temperature, the photocatalytic removal of NOx
950 is regarded as a green and low-cost technology and has attracted much attention.
951 Indeed, some studies have removed or reduced the NOx through clay nanotube
952 systems. For instance, to remove NOx in the presence of UV and Visible light
953 irradiation, Papoulis et al. [224] reported a sol-gel approach for forming
954 TiO_2@halloysite nanocomposites. This was performed under hydrothermal
955 conditions with a halloysite sample from Limnos Island in Greece. The TEM results
956 of the as-prepared nanocomposite exhibited an excellent distribution of TiO_2 on the
957 external surfaces of the halloysite nanotube (**Fig. 20A**). The halloysite acts as a clay
958 stabilizer, preventing the aggregation of nanoparticles because of its substantial
959 specific surface area and its tubular surface [197,198]. The photocatalytic results
960 clearly show that the as-prepared TiO_2@halloysite nanocomposite has significantly
961 better photocatalytic efficiency in decomposing NOx gas when exposed to UV (λ =
962 290 nm) and visible light (λ = 510 nm) illumination: these are, respectively, 2.61 and
963 1.15 times higher than pristine commercial TiO_2 (P25), (**Fig. 20B**). The well-
964 dispersed TiO_2 has explained this higher activity on the halloysite surface. The same
965 research group used the same method to synthesize two TiO_2@halloysite
966 nanocomposites, utilizing halloysite from two distinct geographical regions: Greece
967 and the USA [68]. The two clays showed a good dispersion of TiO_2 NPs in their
968 respective nanocomposites, and both had interparticle mesopores measuring
969 approximately 5.7 nm. It was observed that both nanocomposites demonstrated
970 promising photocatalytic performance for the NOx gas decomposition under visible
971 light (λ = 510 nm) and UV light irradiation (λ = 290 nm) (**Fig. 20C)**. The

TiO_2@halloysite nanocomposite with halloysite from the USA demonstrated higher photocatalytic performance, likely due to its larger specific surface area. (187 m^2/g).

Furthermore, it also revealed considerably improved photocatalytic activity for NOx gas decomposition under visible light (λ = 510 nm) and UV light irradiation (λ = 290 nm), which are, respectively, 9.38 and 1. 69 times higher than pristine commercial TiO_2 (P25) (**Fig. 20C)**. In another study by the same research group [225], a three-phase nanocomposite was prepared using two distinct nanoclay minerals, halloysite, and palygorskite, in combination with TiO_2 (denoted by Hal: PAL-TiO_2) (**Fig. 20D**). The authors demonstrated that the Hal:PAL-TiO_2 nanocomposite exhibited a grey color with enhanced absorption in the visible light region compared to titania P25, which showed no absorption in the same region. The photocatalytic activity of theses systems was further evaluated in this system by decomposing the NOX gas as a function of irradiation time. The results demonstrated that the Hal:PAL-TiO_2 nanocomposite displayed significantly higher activity than the commercial TiO_2 P25 under both UV and visible light irradiation, with up to 8 times higher efficiency under UV light and 1.72 times higher efficiency under visible light (**Fig. 20E)**.

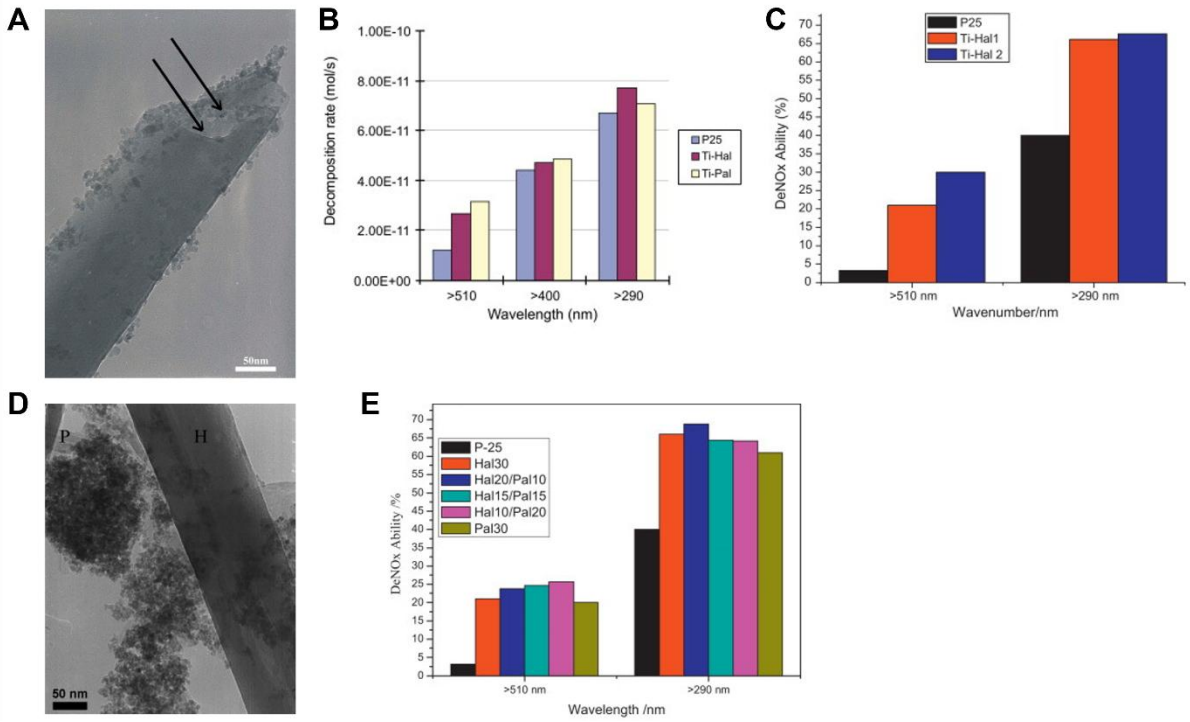

Fig. 20. **A) T**EM images showing TiO_2 grains of about 3–15 nm on halloysite tubes **B**) Photocatalytic activities in decomposing NOx gas by commercial titania P25, TiO_2-treated halloysite (Ti-Hal) and TiO_2-treated palygorskite. Reproduced with permission from [224], Copyright (2010) Elsevier. **C**) Photocatalytic activities in decomposing NOx gas by commercial titania P25, TiO2-treated halloysite (from Greece) and TiO_2-treated halloysite (from USA). Reproduced with permission from [68], Copyright (2013) Elsevier. **D**) TEM micrographs showing the three-phase nanocomposites Hal10:Pal20-TiO_2. **E**) Photocatalytic activity for NOx gas decomposition by commercial titania (P25), single clay–TiO_2, and three-phase nanocomposites. Reproduced with permission from [225], Copyright (2014) Elsevier.

4.4. Photocatalytic disinfection of bacteria

Disinfection of bacteria is of particular importance. Numerous efforts have been dedicated to developing environmentally friendly technologies for disinfecting microorganisms in water [226–228]. However, despite traditional water disinfection technologies such as ozone, chlorination, and ultraviolet methods, they have many disadvantages. For example, they may be chemically or energy-demanding and produce toxic by-products. Photocatalytic disinfection of bacteria, on the other hand, is a non-toxic and eco-friendly process that does not create any harmful by-products.

Escherichia coli is a reliable indicator of water quality concerns within the diverse spectrum of bacteria, often signaling potential fecal contamination due to its presence [226]. The performance of nanotube clay photocatalysts in such applications has been recently investigated. For instance, Xu et al. [210] successfully synthesized a novel composite consisting of Ag/AgBr/halloysite nanotube via a facile sol-gel method and used it to kill gram-negative bacterium *E. Coli* when exposed to visible light. This study's findings revealed that all Ag/AgBr/halloysite nanocomposites exhibited strong absorption in the range of 300 to 1000 nm (**Fig. 21A**). Furthermore, according to the PL spectrum, the Ag/AgBr/halloysite nanotube emitted relatively weak light compared to Ag/AgBr alone, signifying higher separation of the photoexcited electron-hole pairs in the composites and indicating enhanced photocatalytic activity. According to the findings of this study, it was found that when the bacteria was treated with 45% Ag/AgBr/halloysite nanotube composite under irradiation, up to 98% of *E. Coli* was killed, surpassing the efficacy of Ag/AgBr alone under the same conditions (**Fig. 21B and 21C**). Based on this study's experimental observation and characterization results, the formation of the composite is the key factor behind the increased photocatalytic disinfection of bacteria.

In the presence of the Ag/AgBr/halloysite nanotube composite, the photocatalytic mechanisms are as follows: first, the halloysite nanotube serves as the supporting structure in the composite, preventing the decomposition ofAg/AgBr particles; then, the charged surface of the halloysite efficiently improves the separation of electron-hole pairs and promotes the adsorption of *E. Coli*.

The earlier studies show that halloysite has received considerable attention as a photocatalyst. However, it is essential to highlight that research concerning the use of imogolite or chrysotile for photocatalytic bacterial disinfection has been scarcely

explored. This is not so surprising in the case of chrysotile since these nanotubes are known to be toxic, limiting their use. For imogolite nanotubes, some research groups have explored their potential for treating pathogenic bacteria without employing photocatalysis techniques [229,230]. While these investigations represent a valuable exploration of imogolite's antimicrobial properties, they also emphasize the need for additional research to unlock its full potential for combating bacterial contamination.

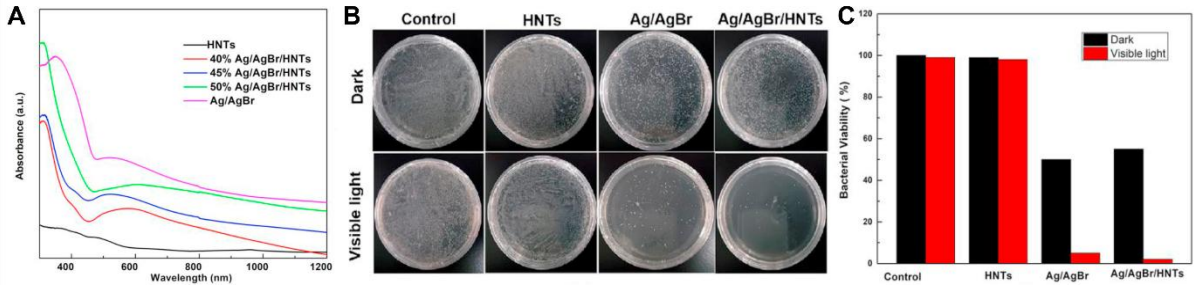

Fig. 21. **A)** UV–Vis absorption spectra of Ag/AgBr/Halloysite nanotube nanocomposite. **B**) Photographs of colonies of E. coli treated with HNTs, Ag/AgBr, and 45%Ag/AgBr/HNTs without and with visible light irradiation, respectively; **C**) Histograms of E. coli viability. Reproduced with permission from [210], Copyright (2021) Elsevier.

5. Conclusion and future perspectives

Nanosized tubular clay materials have garnered significant interest due to their distinctive physicochemical characteristics. The most representative examples of tubular clay materials are imogolite, halloysite, and chrysotile. Although these clays have similar morphology, their chemical structure and properties differ.

Considering that these nanotubular clay materials have a high surface area arising from their nanotubular structure, large pore volumes, higher adsorption capacity, and good mechanical properties, they could offer a wide range of promising applications in photocatalysis. Moreover, these tubular clays also serve as easily

obtainable and low-cost supports to prevent the aggregation of semiconductor materials. However, the only drawback of using these materials as photocatalysts is their wide band gap, which limits their potential in photocatalytic reactions.

Thus, the primary aim of this review has been to compile an extensive overview over several decades, including the recent trends in the development of imogolite, halloysite, and chrysotile, as well as their main physicochemical properties. Furthermore, we have systemically provided an overview of current research progress on these materials for photocatalytic applications, mainly focusing on their intrinsic merits and the challenging aspects of photocatalysis. This review has also elucidated their versatile photocatalytic applications, including the decomposition of organic dye contaminants, selective organic transformation via photocatalysis, hydrogen generation, bacterium disinfection, and reducing nitrogen oxide (NOx) pollution.

Although research has been done on using clay nanotubes as photocatalysts, substrates, or in combination with other photocatalysts in heterogeneous photocatalysis, most investigations in this domain remain in their early stages. Therefore, based on this review, future research should prioritize the following aspects:

(i) Most current research combines imogolite, halloysite, and chrysotile with traditional semiconductors (such as TiO_2 and ZnO). Future research should attempt to combine these clays with new semiconductors. For example, it is possible to develop a co-catalyst without precious metals that can be added to these clay nanotube-based photocatalysts. In addition, the cost should be carefully considered for industrial applications.

(ii) Although numerous studies have examined the photocatalytic capabilities of clay nanotube-based nanocomposites in degrading dye pollutants, most of these works have focused solely on MB, RhB, TC, and MO dyes. Therefore, it is imperative to extend the range of organic pollutants like antibiotics, drug components, and pesticides to assess the photocatalytic degradation potential of such materials comprehensively.

(iii) This review also recommends using actual polluted water instead of simulated wastewater and emphasizes the importance of measuring degradation efficiency through parameters such as TOC removal percentage. Standardization of measurements is also desirable in order to compare the different systems, particularly in terms of stability.

(iv) Undoubtedly, there is a substantial need for in-depth research to elucidate the detailed photocatalytic mechanism of clay nanotubes. This requires the utilization of innovative characterization and computational methods, including but not limited to density functional theory (DFT). Such investigations are crucial for enhancing our understanding of these materials and their photocatalytic processes. There are many more photocatalytic experiments in reducing CO_2 in the presence of imogolite, halloysite, and chrysotile that can be done. This research field seems promising and, to our knowledge, has not yet been investigated by any researcher, nor has there been any published data.

(vi) Future experimental research will be motivated by imogolite's potential to improve polarization in photocatalytic applications, given its natural polarizability and ease of manufacture. This implies that imogolite will soon be used for energy conversion, adding a new substance to the vast field of photocatalysis.

(vii) The current research on imogolite, halloysite, and chrysotile photocatalysts predominantly centers around small-scale laboratory investigations. The focus should shift towards creating environmentally friendly large-scale preparation methods in the future.

Compared to similar nanotube materials, like CNTs, the current study of clay nanotube photocatalysts still needs to be improved. From the number of applications reported in our review article, we conclude that halloysite, chrysotile, and imogolite are versatile materials that can provide new opportunities and directions in the field of photocatalysis.

Acknowledgment:

This work is supported by “Investissements d’Avenir” LabEx PALM (ANR-10-LABX-0039-PALM, project SP3).

References

[1] Saidur R, Abdelaziz EA, Demirbas A, Hossain MS, Mekhilef S. A review on biomass as a fuel for boilers. Renew Sustain Energy Rev 2011;15:2262–89. https://doi.org/10.1016/j.rser.2011.02.015.

[2] Ajmal Z, Naciri Y, Hsini A, Bresolin BM, Qadeer A, Muhammad Nauman MA, et al. Prospects of Photocatalysis in the Management of Nitrate Contamination in Potable Water. 2021. https://doi.org/https://doi.org/10.1007/978-3-030-70757-6_7.

[3] Bouziani A, Yahya M, Naciri Y, Hsini A, Khan MA, Sillanpää M, et al. Development of polyaniline coated titania-hematite composite with enhanced photocatalytic activity under sun-like irradiation. Surfaces and Interfaces 2022;34:102328. https://doi.org/10.1016/J.SURFIN.2022.102328.

[4] Tanji K, El Mrabet I, Fahoul Y, Jellal I, Benjelloun M, Belghiti M, et al. Epigrammatic progress on the photocatalytic properties of ZnO and TiO2 based hydroxyapatite@photocatlyst toward organic molecules photodegradation: A review. J Water Process Eng 2023;53:103682. https://doi.org/10.1016/J.JWPE.2023.103682.

[5] Li J, Jiménez-Calvo P, Paineau E, Ghazzal MN. Metal chalcogenides based heterojunctions and novel nanostructures for photocatalytic hydrogen evolution. Catalysts 2020;10. https://doi.org/10.3390/catal10010089.

[6] Li A, Zhu W, Li C, Wang T, Gong J. Rational design of yolk-shell nanostructures for photocatalysis. Chem Soc Rev 2019;48:1874–907. https://doi.org/10.1039/c8cs00711j.

[7] Zhang T, Wang T, Meng F, Yang M, Kawi S. Recent advances in ZnIn2S4-based materials towards photocatalytic purification, solar fuel production and organic transformations. J Mater Chem C 2022;10:5400–24. https://doi.org/10.1039/d2tc00432a.
[8] UNDP. World Energy Assessment. Energy and the challenge of Sustainability. 2000. https://doi.org/10.1109/ICEE.2017.7893438.
[9] Jiménez-Calvo P, Caps V, Ghazzal MN, Colbeau-Justin C, Keller V. Au/TiO2(P25)-gC3N4 composites with low gC3N4 content enhance TiO2 sensitization for remarkable H2 production from water under visible-light irradiation. Nano Energy 2020;75. https://doi.org/10.1016/j.nanoen.2020.104888.
[10] Wong WY, Ho CL. Organometallic photovoltaics: A new and versatile approach for harvesting solar energy using conjugated polymetallaynes. Acc Chem Res 2010;43:1246–56. https://doi.org/10.1021/ar1000378.
[11] Pinel P, Cruickshank CA, Beausoleil-Morrison I, Wills A. A review of available methods for seasonal storage of solar thermal energy in residential applications. Renew Sustain Energy Rev 2011;15:3341–59. https://doi.org/10.1016/j.rser.2011.04.013.
[12] El-Khouly ME, El-Mohsnawy E, Fukuzumi S. Solar energy conversion: From natural to artificial photosynthesis. J Photochem Photobiol C Photochem Rev 2017;31:36–83. https://doi.org/10.1016/j.jphotochemrev.2017.02.001.
[13] Wang YC, Liu XY, Wang XX, Cao MS. Metal-organic frameworks based photocatalysts: Architecture strategies for efficient solar energy conversion. Chem Eng J 2021;419. https://doi.org/10.1016/j.cej.2021.129459.
[14] Li J, Slassi A, Han X, Cornil D, Ha-Thi MH, Pino T, et al. Tuning the Electronic Bandgap of Graphdiyne by H-Substitution to Promote Interfacial Charge Carrier Separation for Enhanced Photocatalytic Hydrogen Production. Adv Funct Mater 2021;31. https://doi.org/10.1002/adfm.202100994.
[15] Xu Q, Knezevic M, Laachachi A, Franger S, Colbeau-Justin C, Ghazzal MN. Insight into Interfacial Charge Transfer during Photocatalytic H2 Evolution through Fe, Ni, Cu and Au Embedded in a Mesoporous TiO2@SiO2 Core-shell. ChemCatChem 2022. https://doi.org/10.1002/cctc.202200102.
[16] Cui Z, Zhao M, Li S, Wang J, Xu Y, Ghazzal MN, et al. Facile Vacuum Annealing of TiO2with Ethanol-Induced Enhancement of Its Photocatalytic Performance under Visible Light. Ind Eng Chem Res 2022;61:14455–61. https://doi.org/10.1021/acs.iecr.2c01842.
[17] Wang C, Li J, Paineau E, Remita H, Ghazzal MN. Pt Atomically Dispersed in Black TiO2−x/CuxO with Chiral-Like Nanostructure for Visible-Light H2 Generation. Sol RRL 2023;7. https://doi.org/10.1002/solr.202200929.
[18] Tanji K, Zouheir M, Hachhach M, Ahmoum H, Jellal I, Masaoudi H El, et al. Design and simulation of a photocatalysis reactor for rhodamine B degradation using cobalt-doped ZnO film. React Kinet Mech Catal 2021;134:1017–1038. https://doi.org/https://doi.org/10.1007/s11144-021-02116-3.
[19] Fahoul Y, Tanji K, Zouheir M, Mrabet I El, Naciri Y, Hsini A, et al. Novel River Sediment@ZnO@Co nanocomposite for photocatalytic degradation and COD reduction of crystal violet under visible light. J Mol Struct 2022;1253:132298. https://doi.org/10.1016/j.molstruc.2021.132298.
[20] Tanji K, Zouheir M, Naciri Y, Ahmoum H, Hsini A, Mertah O, et al. Visible light photodegradation of blue basic 41 using cobalt doped ZnO: Box–Behnken optimization and DFT calculation. J Iran Chem Soc 2022:1–16. https://doi.org/10.1007/s13738-022-02496-w.

[21] Hamza MA, El-Sayed A, El-Shazly AN, Elmahgary MG. Efficient utilization of ceramic waste (cyclone dust waste) for enhancing the photocatalytic performance of TiO2 nanoparticles toward Rhodamine B photodegradation. J Clean Prod 2024;434:140341. https://doi.org/10.1016/j.jclepro.2023.140341.
[22] Hamza MA, Rizk SA, Ezz-Elregal E-EM, El-Rahman SAA, Ramadan SK, Abou- Gamra ZM. Photosensitization of TiO2 microspheres by novel Quinazoline-derivative as visible-light-harvesting antenna for enhanced Rhodamine B photodegradation. Sci Rep 2023;13:12929. https://doi.org/10.1038/s41598-023-38497-9.
[23] Hamza MA, Abd El-Rahman SA, Abou-Gamra ZM. Facile one-pot solid-state fabrication of a novel binary nanocomposite of commercial ZnO and commercial PbCrO4 with enhanced photocatalytic degradation of Rhodamine B dye. Opt Mater (Amst) 2022;124:111987. https://doi.org/10.1016/j.optmat.2022.111987.
[24] Hashem EM, Hamza MA, El-Shazly AN, Abd El-Rahman SA, El-Tanany EM, Mohamed RT, et al. Novel Z-Scheme/Type-II CdS@ZnO/g-C3N4 ternary nanocomposites for the durable photodegradation of organics: Kinetic and mechanistic insights. Chemosphere 2021;277:128730. https://doi.org/10.1016/j.chemosphere.2020.128730.
[25] Tanji K, El Mrabet I, Fahoul Y, Soussi A, Belghiti M, Jellal I, et al. Experimental and theoretical investigation of enhancing the photocatalytic activity of Mg doped ZnO for nitrophenol degradation. React Kinet Mech Catal 2023;136:1125–42. https://doi.org/10.1007/s11144-023-02385-0.
[26] Zhang Y, Shi Z, Gu Z, Iijima S. Structure modification of single-wall carbon nanotubes. Carbon N Y 2000;38:2055–9. https://doi.org/https://doi.org/10.1016/S0008-6223(00)00047-6.
[27] Ge M, Li Q, Cao C, Huang J, Li S, Zhang S, et al. One-dimensional TiO2 Nanotube Photocatalysts for Solar Water Splitting. Adv Sci 2017;4. https://doi.org/10.1002/advs.201600152.
[28] Ju L, Dai Y, Wei W, Li M, Liang Y, Huang B. One-dimensional cadmium sulphide nanotubes for photocatalytic water splitting. Phys Chem Chem Phys 2018;20:1904–13. https://doi.org/10.1039/c7cp06568j.
[29] Dong X, Yang P, Liu Y, Jia C, Wang D, Wang J, et al. Morphology evolution of one-dimensional ZnO nanostructures towards enhanced photocatalysis performance. Ceram Int 2016;42:518–26. https://doi.org/10.1016/j.ceramint.2015.08.140.
[30] Zhukovskii YF, Piskunov S, Lisovski O, Bocharov D, Evarestov RA. Doped 1D Nanostructures of Transition-metal Oxides: First-principles Evaluation of Photocatalytic Suitability. Isr J Chem 2017;57:461–76. https://doi.org/10.1002/ijch.201600099.
[31] Weng B, Liu S, Zhang N, Tang ZR, Xu YJ. A simple yet efficient visible-light-driven CdS nanowires-carbon nanotube 1D-1D nanocomposite photocatalyst. J Catal 2014;309:146–55. https://doi.org/10.1016/j.jcat.2013.09.013.
[32] Zhang G, Guan Z, Yang J, Li Q, Zhou Y, Zou Z. Metal Sulfides for Photocatalytic Hydrogen Production: Current Development and Future Challenges. Sol RRL 2022;6:1–15. https://doi.org/10.1002/solr.202200587.
[33] Liu Z, Zhang X, Jiang Z, Chen HS, Yang P. Phosphorus and sulphur co-doping of g-C3N4 nanotubes with tunable architectures for superior photocatalytic H2 evolution. Int J Hydrogen Energy 2019;44:20042–55. https://doi.org/10.1016/j.ijhydene.2019.06.037.
[34] Huang K, Li C, Zhang X, Wang L, Wang W, Meng X. Self-assembly synthesis

of phosphorus-doped tubular g-C3N4/Ti3C2 MXene Schottky junction for boosting photocatalytic hydrogen evolution. Green Energy Environ 2021. https://doi.org/10.1016/j.gee.2021.03.011.
[35] Kumar S, Sharma M, Powar S, Kabachkov EN, Vaish R. Impact of remnant surface polarization on photocatalytic and antibacterial performance of BaTiO 3. J Eur Ceram Soc 2019;39:2915–22. https://doi.org/10.1016/j.jeurceramsoc.2019.03.029.
[36] Ali SS, Qazi IA, Arshad M, Khan Z, Voice TC, Mehmood CT. Photocatalytic degradation of low density polyethylene (LDPE) films using titania nanotubes. Environ Nanotechnology, Monit Manag 2016;5:44–53. https://doi.org/10.1016/j.enmm.2016.01.001.
[37] Sun L, Li J, Wang C, Li S, Lai Y, Chen H, et al. Ultrasound aided photochemical synthesis of Ag loaded TiO2 nanotube arrays to enhance photocatalytic activity. J Hazard Mater 2009;171:1045–50. https://doi.org/10.1016/j.jhazmat.2009.06.115.
[38] Das R, Abd Hamid SB, Ali ME, Ismail AF, Annuar MSM, Ramakrishna S. Multifunctional carbon nanotubes in water treatment: The present, past and future. Desalination 2014;354:160–79. https://doi.org/10.1016/j.desal.2014.09.032.
[39] Liu X, Wang M, Zhang S, Pan B. Application potential of carbon nanotubes in water treatment: A review. J Environ Sci (China) 2013;25:1263–80. https://doi.org/10.1016/S1001-0742(12)60161-2.
[40] Zhang X, Zhang X, Yang P, Ping Jiang S. Transition metals decorated g-C3N4/N-doped carbon nanotube catalysts for water splitting: A review. J Electroanal Chem 2021;895. https://doi.org/10.1016/j.jelechem.2021.115510.
[41] Lvov Y, Wang W, Zhang L, Fakhrullin R. Halloysite Clay Nanotubes for Loading and Sustained Release of Functional Compounds. Adv Mater 2016;28:1227–50. https://doi.org/10.1002/adma.201502341.
[42] Paineau E, Bihannic I, Baravian C, Philippe AM, Davidson P, Levitz P, et al. Aqueous suspensions of natural swelling clay minerals. 1. structure and electrostatic interactions. Langmuir 2011;27:5562–73. https://doi.org/10.1021/la2001255.
[43] Paineau E, Rouzière S, Monet G, Diogo CC, Morfin I, Launois P. Role of initial precursors on the liquid-crystalline phase behavior of synthetic aluminogermanate imogolite nanotubes. J Colloid Interface Sci 2020;580:275–85. https://doi.org/10.1016/j.jcis.2020.07.036.
[44] Serra M, Arenal R, Tenne R. An overview of the recent advances in inorganic nanotubes. Nanoscale 2019;11:8073–90. https://doi.org/10.1039/c9nr01880h.
[45] Liu Q, Peng H, Tian X, Guo J. Synthesis of chrysotile based nanocomposites for tuning band gap and photocatalytic property. Appl Clay Sci 2020;199. https://doi.org/10.1016/j.clay.2020.105885.
[46] Liu M, Chang Y, Yang J, You Y, He R, Chen T, et al. Functionalized halloysite nanotube by chitosan grafting for drug delivery of curcumin to achieve enhanced anticancer efficacy. J Mater Chem B 2016;4:2253–63. https://doi.org/10.1039/c5tb02725j.
[47] Luo Q, Peng H, Tian X, Guo J. Facile synthesis and characterization of Chrysotile/SnO2 nanocomposite for enhanced photocatalytic properties. Appl Organomet Chem 2020;34. https://doi.org/10.1002/aoc.5356.
[48] Joussein, E. Petit, S.Churchman, J.Theng, B. Righi, D. And Delvaux B. Halloysite clay minerals- a review. Clay Miner 2005;40:383–426. https://doi.org/https://doi.org/10.1180/0009855054040180.

[49] Liu M, Chang Y, Yang J, You Y, He R, Chen T, et al. Functionalized halloysite nanotube by chitosan grafting for drug delivery of curcumin to achieve enhanced anticancer efficacy. J Mater Chem B 2016;4:2253–63. https://doi.org/10.1039/c5tb02725j.
[50] Yuan P, Tan D, Annabi-Bergaya F. Properties and applications of halloysite nanotubes: Recent research advances and future prospects. Appl Clay Sci 2015;112–113:75–93. https://doi.org/10.1016/j.clay.2015.05.001.
[51] Gonza RI, Ram R, Rogan J, Valdivia JA, Munoz F, Valencia F, et al. Model for Self-Rolling of an Aluminosilicate Sheet into a Single- Walled Imogolite Nanotube. J Phys Chem C 2014;118:28227. https://doi.org/https://doi.org/10.1021/jp508637q.
[52] P. D. G. Cradwick, V. C. Farmer, J. D. Russel, C. R. Masson KW& NY. Imogolite, a Hydrated Aluminium Silicate of Tubular Structure. Nat Phys Sci 1972;240:187–9. https://doi.org/https://doi.org/10.1038/physci240187a0.
[53] Paineau E. Imogolite nanotubes: A flexible nanoplatform with multipurpose applications. Appl Sci 2018;8. https://doi.org/10.3390/app8101921.
[54] D'Angelo A, Paineau E, Rouzière S, Elkaim É, Goldmann C, Toquer D, et al. The atomic structure of imogolite nanotubes: A 50 years old issue reinvestigated by X-ray scattering experiments and molecular dynamics simulations. Appl Clay Sci 2023;242:107043. https://doi.org/10.1016/j.clay.2023.107043.
[55] King TVV, Clark RN. Spectral characteristics of chlorites and Mg-serpentines using high- resolution reflectance spectroscopy. J Geophys Res 1989;94. https://doi.org/10.1029/jb094ib10p13997.
[56] Krasilin AA. energy modeling of competition between tubular and platy morphologies of chrysotile and halloysite layers. Clays Clay Miner 2020;68:436–45. https://doi.org/10.1007/s42860-020-00086-6.
[57] Teobaldi G, Beglitis NS, Fisher AJ, Zerbetto F, Hofer WA. Hydroxyl vacancies in single-walled aluminosilicate and aluminogermanate nanotubes. J Phys Condens Matter 2009;21. https://doi.org/10.1088/0953-8984/21/19/195301.
[58] Guimarães L, Enyashin AN, Frenzel J, Heine T, Duarte HA, Seifert G. Imogolite nanotubes: Stability, electronic, and mechanical properties. ACS Nano 2007;1:362–8. https://doi.org/10.1021/nn700184k.
[59] Piperno S, Kaplan-Ashiri I, Cohen SR, Popovitz-Biro R, Wagner HD, Tenne R, et al. Characterization of geoinspired and synthetic chrysotile nanotubes by atomic force microscopy and transmission electron microscopy. Adv Funct Mater 2007;17:3332–8. https://doi.org/10.1002/adfm.200700278.
[60] Lecouvet B, Horion J, D'Haese C, Bailly C, Nysten B. Elastic modulus of halloysite nanotubes. Nanotechnology 2013;24. https://doi.org/10.1088/0957-4484/24/10/105704.
[61] S.Rouzière, V. Balédent, E. Paineau, E. Elkaim, T. Bizien, L. Nataf, Y. Pan and PL. Compressibility and Structural Transformations of Aluminogermanate Imogolite Nanotubes under Hydrostatic Pressure. Inorg Chem 2023;62:957-966. https://doi.org/https://doi.org/10.1021/acs.inorgchem.2c03798.
[62] Xiao M, Wang Z, Lyu M, Luo B, Wang S, Liu G, et al. Hollow Nanostructures for Photocatalysis: Advantages and Challenges. Adv Mater 2019;31. https://doi.org/10.1002/adma.201801369.
[63] Alvarez-Ramírez F. First principles studies of Fe-containing aluminosilicate and aluminogermanate nanotubes. J Chem Theory Comput 2009;5:3224–31. https://doi.org/10.1021/ct9004992.
[64] Zhao M, Xia Y, Mei L. Energetic minimum structures of imogolite nanotubes: A

first-principles prediction. J Phys Chem C 2009;113:14834–7. https://doi.org/10.1021/jp9056169.
[65] Poli E, Elliott JD, Ratcliff LE, Andrinopoulos L, Dziedzic J, Hine NDM, et al. The potential of imogolite nanotubes as (co-)photocatalysts: A linear-scaling density functional theory study. J Phys Condens Matter 2016;28:074003. https://doi.org/10.1088/0953-8984/28/7/074003.
[66] Pignié MC, Shcherbakov V, Charpentier T, Moskura M, Carteret C, Denisov S, et al. Confined water radiolysis in aluminosilicate nanotubes: The importance of charge separation effects. Nanoscale 2021;13:3092–105. https://doi.org/10.1039/d0nr08948f.
[67] Katsumata K ichi, Hou X, Sakai M, Nakajima A, Fujishima A, Matsushita N, et al. Visible-light-driven photodegradation of acetaldehyde gas catalyzed by aluminosilicate nanotubes and Cu(II)-grafted TiO2 composites. Appl Catal B Environ 2013;138–139:243–52. https://doi.org/10.1016/j.apcatb.2013.03.004.
[68] Papoulis D, Komarneni S, Panagiotaras D, Stathatos E, Toli D, Christoforidis KC, et al. Halloysite-TiO2 nanocomposites: Synthesis, characterization and photocatalytic activity. Appl Catal B Environ 2013;132–133:416–22. https://doi.org/10.1016/j.apcatb.2012.12.012.
[69] Monteiro RRC, de Oliveira ALB, de Menezes FL, de Souza MCM, Fechine PBA, dos Santos JCS. Improvement of enzymatic activity and stability of lipase A from Candida antartica onto halloysite nanotubes with Taguchi method for optimized immobilization. Appl Clay Sci 2022;228. https://doi.org/10.1016/j.clay.2022.106634.
[70] Barebita H, Naciri Y, Ferraa S, Nimour A, Guedira T. Investigation of structural and photocatalytic behavior of Bi13B1-2xVxPxO20. 95+ 2x (0≤ x≤ 0.5). Solid State Sci 2020;108:106389. https://doi.org/https://doi.org/10.1016/j.solidstatesciences.2020.106389.
[71] Naciri Y, Hsini A, Bouziani A, Tanji K, El Ibrahimi B, Ghazzal MN, et al. Z-scheme WO3/PANI heterojunctions with enhanced photocatalytic activity under visible light: A depth experimental and DFT studies. Chemosphere 2022;292:133468. https://doi.org/10.1016/j.chemosphere.2021.133468.
[72] Naciri Y, Hsini A, Bouziani A, Djellabi R, Ajmal Z, Laabd M, et al. Photocatalytic oxidation of pollutants in gas-phase via Ag3PO4-based semiconductor photocatalysts: Recent progress, new trends, and future perspectives. Crit Rev Environ Sci Technol 2022;52:2339–82. https://doi.org/10.1080/10643389.2021.1877977.
[73] Ran J, Jaroniec M, Qiao SZ. Cocatalysts in Semiconductor-based Photocatalytic CO2 Reduction: Achievements, Challenges, and Opportunities. Adv Mater 2018;30. https://doi.org/10.1002/adma.201704649.
[74] Zhou P, Yu J, Jaroniec M. All-solid-state Z-scheme photocatalytic systems. Adv Mater 2014;26:4920–35. https://doi.org/10.1002/adma.201400288.
[75] Rahman MZ, Kibria MG, Mullins CB. Metal-free photocatalysts for hydrogen evolution. Chem Soc Rev 2020;49:1887–931. https://doi.org/10.1039/c9cs00313d.
[76] Kudo A, Miseki Y. Heterogeneous photocatalyst materials for water splitting. Chem Soc Rev 2009;38:253–78. https://doi.org/10.1039/b800489g.
[77] Wang Q, Domen K. Particulate Photocatalysts for Light-Driven Water Splitting: Mechanisms, Challenges, and Design Strategies. Chem Rev 2020;120:919–85. https://doi.org/10.1021/acs.chemrev.9b00201.
[78] Naciri Y, Hsini A, Ajmal Z, Navío JA, Bakiz B, Albourine A, et al. Recent progress on the enhancement of photocatalytic properties of BiPO4 using π–

conjugated materials. Adv Colloid Interface Sci 2020;280. https://doi.org/10.1016/j.cis.2020.102160.
[79] Naciri Y, Hsini A, Ahdour A, Akhsassi B, Fritah kamal, Ajmal Z, et al. Recent advances of bismuth titanate based photocatalysts engineering for enhanced organic contaminates oxidation in water: A review. Chemosphere 2022;300. https://doi.org/10.1016/j.chemosphere.2022.134622.
[80] Fahoul Y, Tanji K, González Díaz OM, Quesada-Cabrera R, Naciri Y, El Mrabet I, et al. Development of a new CoS-Supported ZnAl2O4 catalyst for the visible photodegradation of a basic textile dye from water. Opt Mater (Amst) 2023;143. https://doi.org/10.1016/j.optmat.2023.114148.
[81] Kubacka A, Fernández-García M, Colón G. Advanced nanoarchitectures for solar photocatalytic applications. Chem Rev 2012;112:1555–614. https://doi.org/10.1021/cr100454n.
[82] Wei K, Faraj Y, Yao G, Xie R, Lai B. Strategies for improving perovskite photocatalysts reactivity for organic pollutants degradation: A review on recent progress. Chem Eng J 2021;414. https://doi.org/10.1016/j.cej.2021.128783.
[83] Hu C, Tu S, Tian N, Ma T, Zhang Y, Huang H. Photocatalysis Enhanced by External Fields. Angew Chemie - Int Ed 2021;60:16309–28. https://doi.org/10.1002/anie.202009518.
[84] Mimouni I, Yahya M, Bouziani A, Naciri Y, Maarouf F ezzahra, Alaoui El Belghiti M, et al. Iron phosphate for photocatalytic removal of Ibuprofen from aqueous media under sun-like irradiation. J Photochem Photobiol A Chem 2022;433:114170. https://doi.org/10.1016/j.jphotochem.2022.114170.
[85] Ajmal Z, Naciri Y, Ahmad M, Hsini A, Bouziani A, Laabd M, et al. Use of conductive polymer-supported oxide-based photocatalysts for efficient VOCs & SVOCs removal in gas/liquid phase. J Environ Chem Eng 2023;11:108935. https://doi.org/10.1016/j.jece.2022.108935.
[86] Akhsassi B, Naciri Y, Bouddouch A, Bakiz B, Taoufyq A, Villain S, et al. Facile novel acid coprecipitation synthesis of BiPO4 polymorphs: Enhanced photocatalytic degradation of the antibiotic AMX and the dyes RhB, MB and MO. Opt Mater (Amst) 2023;137:113575. https://doi.org/10.1016/j.optmat.2023.113575.
[87] Sadjadi S. Halloysite-based hybrids/composites in catalysis. Appl Clay Sci 2020;189. https://doi.org/10.1016/j.clay.2020.105537.
[88] Mishra A, Mehta A, Basu S. Clay supported TiO2 nanoparticles for photocatalytic degradation of environmental pollutants: A review. J Environ Chem Eng 2018;6:6088–107. https://doi.org/10.1016/j.jece.2018.09.029.
[89] Li C, Zhu N, Yang S, He X, Zheng S, Sun Z, et al. A review of clay based photocatalysts: Role of phyllosilicate mineral in interfacial assembly, microstructure control and performance regulation. Chemosphere 2021;273:129723. https://doi.org/10.1016/j.chemosphere.2021.129723.
[90] Zhu S, Wang D. Photocatalysis: Basic principles, diverse forms of implementations and emerging scientific opportunities. Adv Energy Mater 2017;7:1–24. https://doi.org/10.1002/aenm.201700841.
[91] Xiao FX, Miao J, Tao HB, Hung SF, Wang HY, Yang H Bin, et al. One-dimensional hybrid nanostructures for heterogeneous photocatalysis and photoelectrocatalysis. Small 2015;11:2115–31. https://doi.org/10.1002/smll.201402420.
[92] Li L, Zhao C, Zhang L, Zhu Y. γ-GeSe nanotubes: A one-dimensional semiconductor with high carrier mobility potential for photocatalytic water splitting. J Mater Chem C 2021;9:15158–64.

https://doi.org/10.1039/d1tc04204a.
[93] Jiang D, Jing H, Liu Z, Jia C, Liu Q. Natural Halloysite Nanotube as a Spatially Confined Nanoreactor for Improving Photocatalytic Performance. J Phys Chem C 2021;125:15316–23. https://doi.org/10.1021/acs.jpcc.1c04065.
[94] Zhu K, Neale NR, Miedaner A, Frank AJ. Enhanced charge-collection efficiencies and light scattering in dye-sensitized solar cells using oriented TiO2 nanotubes arrays. Nano Lett 2007;7:69–74. https://doi.org/10.1021/nl062000o.
[95] Macak JM, Zlamal M, Krysa J, Schmuki P. Self-organized TiO2 nanotube layers as highly efficient photocatalysts. Small 2007;3:300–4. https://doi.org/10.1002/smll.200600426.
[96] Patra S, Schaming D, Picot P, Pignié MC, Brubach JB, Sicard L, et al. Inorganic nanotubes with permanent wall polarization as dual photo-reactors for wastewater treatment with simultaneous fuel production. Environ Sci Nano 2021;8:2523–41. https://doi.org/10.1039/d1en00405k.
[97] Das S, Jana S. A tubular nanoreactor directing the formation of in situ iron oxide nanorods with superior photocatalytic activity. Environ Sci Nano 2017;4:596–603. https://doi.org/10.1039/c6en00570e.
[98] Zsirka B, Vágvölgyi V, Horváth E, Juzsakova T, Fónagy O, Szabó-bárdos E, et al. Halloysite-Zinc Oxide Nanocomposites as Potential Photocatalysts. Minerals 2022;12. https://doi.org/10.3390/min12040476.
[99] Mishra G, Mukhopadhyay M. TiO2 decorated functionalized halloysite nanotubes (TiO2 @HNTs) and photocatalytic PVC membranes synthesis, characterization and its application in water treatment. Sci Rep 2019;9:1–17. https://doi.org/10.1038/s41598-019-40775-4.
[100] Pignié MC, Patra S, Huart L, Milosavljević AR, Renault JP, Leroy J, et al. Experimental determination of the curvature-induced intra-wall polarization of inorganic nanotubes. Nanoscale 2021;13:19650–62. https://doi.org/10.1039/d1nr06462b.
[101] Chen F, Huang H, Guo L, Zhang Y, Ma T. The Role of Polarization in Photocatalysis. Angew Chemie - Int Ed 2019;58:10061–73. https://doi.org/10.1002/anie.201901361.
[102] Ghicov A, Schmuki P. Self-ordering electrochemistry: A review on growth and functionality of TiO2 nanotubes and other self-aligned MOx structures. Chem Commun 2009:2791–808. https://doi.org/10.1039/b822726h.
[103] Zhang P, Lou XW (David). Design of Heterostructured Hollow Photocatalysts for Solar-to-Chemical Energy Conversion. Adv Mater 2019;31:1–18. https://doi.org/10.1002/adma.201900281.
[104] Wong LW, Goh CBS, Pasbakhsh P, Tan JBL. Natural hollow clay nanotubes and their applications as polymer nanocomposites in tissue engineering. J Sci Adv Mater Devices 2022;7. https://doi.org/10.1016/j.jsamd.2022.100431.
[105] Ng KM, Lau YTR, Chan CM, Weng LT, Wu J. Surface studies of halloysite nanotubes by XPS and ToF-SIMS. Surf Interface Anal 2011;43:795–802. https://doi.org/10.1002/sia.3627.
[106] Cavallaro G, Lazzara G, Konnova S, Fakhrullin R, Lvov Y. Composite films of natural clay nanotubes with cellulose and chitosan. Green Mater 2014;2:232–42. https://doi.org/10.1680/gmat.14.00014.
[107] Abdullayev E, Lvov Y. Halloysite clay nanotubes for controlled release of protective agents. J Nanosci Nanotechnol 2011;11:10007–26. https://doi.org/10.1166/jnn.2011.5724.
[108] Cavallaro G, Lazzara G, Pignon F, Chiappisi L, Paineau E. Effect of Polymer

Length on the Adsorption onto Aluminogermanate Imogolite Nanotubes. Langmuir 2021;37:9858–64. https://doi.org/10.1021/acs.langmuir.1c01549.
[109] Luo P, Zhao Y, Zhang B, Liu J, Yang Y, Liu J. Study on the adsorption of Neutral Red from aqueous solution onto halloysite nanotubes. Water Res 2010;44:1489–97. https://doi.org/10.1016/j.watres.2009.10.042.
[110] Sadjadi S. Halloysite-based hybrids/composites in catalysis. Appl Clay Sci 2020;189:105537. https://doi.org/10.1016/j.clay.2020.105537.
[111] Lazzara G, Cavallaro G, Panchal A, Fakhrullin R, Stavitskaya A, Vinokurov V, et al. An assembly of organic-inorganic composites using halloysite clay nanotubes. Curr Opin Colloid Interface Sci 2018;35:42–50. https://doi.org/10.1016/j.cocis.2018.01.002.
[112] Lisuzzo L, Cavallaro G, Lazzara G, Milioto S, Parisi F, Stetsyshyn Y. Stability of halloysite, imogolite, and boron nitride nanotubes in solvent media. Appl Sci 2018;8. https://doi.org/10.3390/app8071068.
[113] Ferrante F, Armata N, Lazzara G. Modeling of the Halloysite Spiral Nanotube. J Phys Chem C 2015;119:16700–7. https://doi.org/10.1021/acs.jpcc.5b04281.
[114] Joo Y, Joo JH, Jeon Y, Lee SU, Sohn D. Opening and blocking the inner-pores of halloysite. Chem Commun 2013;49:4519–21. https://doi.org/10.1039/c3cc40465j.
[115] Atyaksheva LF, Kasyanov IA. Halloysite, Natural Aluminosilicate Nanotubes: Structural Features and Adsorption Properties (A Review). Pet Chem 2021;61:932–50. https://doi.org/10.1134/S0965544121080119.
[116] Gianni E, Pšenička M, Macková K, Scholtzová E, Jankovič Ľ, Mareš M, et al. New detail insight into Halloysite structure: Mechanism behind nanotubular morphology described by density functional theory and molecular dynamics supported by experiments. J Mol Struct 2023;1287. https://doi.org/10.1016/j.molstruc.2023.135639.
[117] Zhang Y, Fu L, Shu Z, Yang H, Tang A, Jiang T. Substitutional Doping for Aluminosilicate Mineral and Superior Water Splitting Performance. Nanoscale Res Lett 2017;12. https://doi.org/10.1186/s11671-017-2192-8.
[118] Yoshinaga N, Aomine S. Imogolite in some ando soils. Soil Sci Plant Nutr 1962;8:22–9. https://doi.org/10.1080/00380768.1962.10430993.
[119] Paineau E, Launois P. Nanomaterials from imogolite: Structure, properties, and functional materials. Nanomater. from Clay Miner. A New Approach to Green Funct. Mater., Elsevier; 2019, p. 257–84. https://doi.org/10.1016/B978-0-12-814533-3.00005-3.
[120] Garrone E, Bonelli B. Imogolite for Catalysis and Adsorption. Dev. Clay Sci., vol. 7, Elsevier B.V.; 2016, p. 672–707. https://doi.org/10.1016/B978-0-08-100293-3.00025-X.
[121] Konduri S, Mukherjee S, Nair S. Strain energy minimum and vibrational properties of single-walled aluminosilicate nanotubes. Phys Rev B - Condens Matter Mater Phys 2006;74:1–4. https://doi.org/10.1103/PhysRevB.74.033401.
[122] Monet G, Amara MS, Rouzière S, Paineau E, Chai Z, Elliott JD, et al. Structural resolution of inorganic nanotubes with complex stoichiometry. Nat Commun 2018;9. https://doi.org/10.1038/s41467-018-04360-z.
[123] Paineau E, Monet G, Peyre V, Goldmann C, Rouzière S, Launois P. Colloidal Stability of Imogolite Nanotube Dispersions: A Phase Diagram Study. Langmuir 2019;35:12451–9. https://doi.org/10.1021/acs.langmuir.9b01922.
[124] Farmer VC, Fraser AR, Tait. Synthesis of Imogolite: A Tubular Aluminium Silicate Polymer. 1977. https://doi.org/https://doi.org/10.1039/C39770000462.
[125] Farmer VC, Adams MJ, Fraser AR, Palmieri F. Synthetic imogolite: properties,

synthesis and possible applications. Clay Miner 1983;18:459–72. https://doi.org/10.1180/claymin.1983.018.4.11.
[126] Bursill LA, Peng JL, Bourgeois LN. Imogolite: An aluminosilicate nanotube material. Philos Mag A Phys Condens Matter, Struct Defects Mech Prop 2000;80:105–17. https://doi.org/10.1080/01418610008212043.
[127] Li L, Xia Y, Zhao M, Song C, Li J, Liu X. The electronic structure of a single-walled aluminosilicate nanotube. Nanotechnology 2008;19. https://doi.org/10.1088/0957-4484/19/17/175702.
[128] Alvarez-Ramírez F. Ab initio simulation of the structural and electronic properties of aluminosilicate and aluminogermanate natotubes with imogolite-like structure. Phys Rev B - Condens Matter Mater Phys 2007;76. https://doi.org/10.1103/PhysRevB.76.125421.
[129] Kato K, Inukai K, Fujikura K, Kasuga T. Effective encapsulation of laccase in an aluminium silicate nanotube hydrogel. New J Chem 2014;38:3591–9. https://doi.org/10.1039/c4nj00080c.
[130] Wada S-I, Wada K. Effets of substitution of germanium. vol. 30. 1982. https://doi.org/https://doi.org/10.1346/CCMN.1982.0300206.
[131] Paineau E, Krapf MEM, Amara MS, Matskova N V., Dozov I, Rouzière S, et al. A liquid-crystalline hexagonal columnar phase in highly-dilute suspensions of imogolite nanotubes. Nat Commun 2016;7:1–8. https://doi.org/10.1038/ncomms10271.
[132] Amara MS, Paineau E, Bacia-Verloop M, Krapf MEM, Davidson P, Belloni L, et al. Single-step formation of micron long (OH)3Al2O3Ge(OH) imogolite-like nanotubes. Chem Commun 2013;49:11284–6. https://doi.org/10.1039/c3cc46839a.
[133] Maillet P, Levard C, Spalla O, Masion A, Rose J, Thill A. Growth kinetic of single and double-walled aluminogermanate imogolite-like nanotubes: An experimental and modeling approach. Phys Chem Chem Phys 2011;13:2682–9. https://doi.org/10.1039/c0cp01851a.
[134] Bottero I, Bonelli B, Ashbrook SE, Wright PA, Zhou W, Tagliabue M, et al. Synthesis and characterization of hybrid organic/inorganic nanotubes of the imogolite type and their behaviour towards methane adsorption. Phys Chem Chem Phys 2011;13:744–50. https://doi.org/10.1039/c0cp00438c.
[135] Liao YY, Picot P, Brubach JB, Roy P, Thill A, Le Caër S. Water Adsorption in Single- And Double-Walled Inorganic Nanotubes. J Phys Chem C 2019;123:19768–77. https://doi.org/10.1021/acs.jpcc.9b05621.
[136] Amara MS, Paineau E, Rouzière S, Guiose B, Krapf MEM, Taché O, et al. Hybrid, tunable-diameter, metal oxide nanotubes for trapping of organic molecules. Chem Mater 2015;27:1488–94. https://doi.org/10.1021/cm503428q.
[137] Liao Y, Picot P, Brubach JB, Roy P, Le Caër S, Thill A. Self-supporting thin films of imogolite and imogolite-like nanotubes for infrared spectroscopy. Appl Clay Sci 2018;164:58–67. https://doi.org/10.1016/j.clay.2017.06.005.
[138] Kang DY, Brunelli NA, Yucelen GI, Venkatasubramanian A, Zang J, Leisen J, et al. Direct synthesis of single-walled aminoaluminosilicate nanotubes with enhanced molecular adsorption selectivity. Nat Commun 2014;5. https://doi.org/10.1038/ncomms4342.
[139] Wang J, Wang Z, Huang B, Ma Y, Liu Y, Qin X, et al. Oxygen vacancy induced band-gap narrowing and enhanced visible light photocatalytic activity of ZnO. ACS Appl Mater Interfaces 2012;4:4024–30. https://doi.org/10.1021/am300835p.
[140] El-Shamy A gamal. New carbon quantum dots nano-particles decorated zinc

peroxide (Cdots/ZnO2) nano-composite with superior photocatalytic efficiency for removal of different dyes under UV-A light. Synth Met 2020;267:116472. https://doi.org/10.1016/j.synthmet.2020.116472.
[141] Hsu CC, Wu NL. Synthesis and photocatalytic activity of ZnO/ZnO2 composite. J Photochem Photobiol A Chem 2005;172:269–74. https://doi.org/10.1016/j.jphotochem.2004.12.014.
[142] Shafia E, Esposito S, Manzoli M, Chiesa M, Tiberto P, Barrera G, et al. Al/Fe isomorphic substitution versus Fe2O3 clusters formation in Fe-doped aluminosilicate nanotubes (imogolite). J Nanoparticle Res 2015;17. https://doi.org/10.1007/s11051-015-3130-2.
[143] Shafia E, Esposito S, Armandi M, Manzoli M, Garrone E, Bonelli B. Isomorphic substitution of aluminium by iron into single-walled alumino-silicate nanotubes: A physico-chemical insight into the structural and adsorption properties of Fe-doped imogolite. Microporous Mesoporous Mater 2016;224:229–38. https://doi.org/10.1016/j.micromeso.2015.11.044.
[144] Ookawaa M, Inouea Y, Watanabea M, Suzukib M, Yamaguchia T. Synthesis and Characterization of Fe Containing Imogolite. vol. 12. 2006. https://doi.org/https://doi.org/10.11362/jcssjclayscience1960.12.Supplement2_280.
[145] Guimarães L, Pinto YN, Lourenço MP, Duarte HA. Imogolite-like nanotubes: Structure, stability, electronic and mechanical properties of the phosphorous and arsenic derivatives. Phys Chem Chem Phys 2013;15:4303–9. https://doi.org/10.1039/c3cp44250k.
[146] Alvarez-Ramírez F. Theoretical study of (OH)3N2O3MOH, M = C, Si, Ge, Sn and N = Al, Ga, In, with imogolite-like structure. J Comput Theor Nanosci 2009;6:1120–4. https://doi.org/10.1166/jctn.2009.1152.
[147] Poli E, Elliott JD, Chulkov SK, Watkins MB, Teobaldi G. The role of cation-vacancies for the electronic and optical properties of aluminosilicate imogolite nanotubes: A non-local, linear-response TDDFT study. Front Chem 2019;7:1–17. https://doi.org/10.3389/fchem.2019.00210.
[148] Popov IS, Enyashin AN. Imogolite: Curvature-Induced Hospitality for Trivalent Dopants. Phys Status Solidi Basic Res 2021;258:1–9. https://doi.org/10.1002/pssb.202100188.
[149] Li J, Cai L, Shang J, Yu Y, Zhang L. Giant Enhancement of Internal Electric Field Boosting Bulk Charge Separation for Photocatalysis. Adv Mater 2016;28:4059–64. https://doi.org/10.1002/adma.201600301.
[150] Wu Y, Gao Z, Li H, Sun X, Li D, Zhou G, et al. Promoting carrier separation efficiently by macroscopic polarization charges and interfacial modulation for photocatalysis. Chem Eng J 2021;410. https://doi.org/10.1016/j.cej.2020.128393.
[151] Gao Y, Nie W, Zhu Q, Wang X, Wang S, Fan F, et al. The Polarization Effect in Surface-Plasmon-Induced Photocatalysis on Au/TiO2 Nanoparticles. Angew Chemie - Int Ed 2020;59:18218–23. https://doi.org/10.1002/anie.202007706.
[152] Dong XD, Yao GY, Liu QL, Zhao QM, Zhao ZY. Spontaneous Polarization Effect and Photocatalytic Activity of Layered Compound of BiOIO3. Inorg Chem 2019;58:15344–53. https://doi.org/10.1021/acs.inorgchem.9b02328.
[153] Gustafsson JP. The surface chemistry of imogolite. Clays Clay Miner n.d.;49:73–80. https://doi.org/https://doi.org/10.1346/CCMN.2001.0490106.
[154] Elliott JD, Poli E, Scivetti I, Ratcliff LE, Andrinopoulos L, Dziedzic J, et al. Chemically Selective Alternatives to Photoferroelectrics for Polarization-Enhanced Photocatalysis: The Untapped Potential of Hybrid Inorganic

Nanotubes. Adv Sci 2017;4. https://doi.org/10.1002/advs.201600153.
[155] Bonelli B, Armandi M, Garrone E. Surface properties of alumino-silicate single-walled nanotubes of the imogolite type. Phys Chem Chem Phys 2013;15:13381–90. https://doi.org/10.1039/c3cp51508g.
[156] Zanzottera C, Vicente A, Celasco E, Fernandez C, Garrone E, Bonelli B. Physico-chemical properties of imogolite nanotubes functionalized on both external and internal surfaces. J Phys Chem C 2012;116:7499–506. https://doi.org/10.1021/jp301177q.
[157] Patra S, Testard F, Gobeaux F, Sicard L, Shaming D, Caër S Le, et al. UV-Visible photo-reactivity of permanently polarized inorganic nanotubes coupled to gold nanoparticles. Nanoscale 2023;15:4101–13. https://doi.org/10.1039/d2nr05796d.
[158] Kanarek MS. Mesothelioma from Chrysotile Asbestos: Update. Ann Epidemiol 2011;21:688–97. https://doi.org/10.1016/j.annepidem.2011.05.010.
[159] Bernstein D, Dunnigan J, Hesterberg T, Brown R, Velasco JAL, Barrera R, et al. Health risk of chrysotile revisited. Crit Rev Toxicol 2013;43:154–83. https://doi.org/10.3109/10408444.2012.756454.
[160] Bernstein DM, Hoskins JA. The health effects of chrysotile: Current perspective based upon recent data. Regul Toxicol Pharmacol 2006;45:252–64. https://doi.org/10.1016/j.yrtph.2006.04.008.
[161] Mohanty SK, Gonneau C, Salamatipour A, Pietrofesa RA, Casper B, Christofidou-Solomidou M, et al. Siderophore-mediated iron removal from chrysotile: Implications for asbestos toxicity reduction and bioremediation. J Hazard Mater 2018;341:290–6. https://doi.org/10.1016/j.jhazmat.2017.07.033.
[162] Poland CA, Duffin R. The toxicology of chrysotile-containing brake debris: implications for mesothelioma. Crit Rev Toxicol 2019;49:11–35. https://doi.org/10.1080/10408444.2019.1568385.
[163] Keija Yada. Study of Microstructure of Chrysotile Asbestos by High Resolution Electron Microscopy. vol. 12. 1957. https://doi.org/https://doi.org/10.1107/S0567739471001402.
[164] Falini G, Foresti E, Gazzano M, Gualtieri AE, Leoni M, Lesci IG, et al. Tubular-shaped stoichiometric chrysotile nanocrystals. Chem - A Eur J 2004;10:3043–9. https://doi.org/10.1002/chem.200305685.
[165] Pollastri S, Perchiazzi N, Lezzerini M, Plaisier JR, Cavallo A, Dalconi MC, et al. The crystal structure of mineral fibres. 1. Chrysotile. Period Di Mineral 2016;85:249–59. https://doi.org/10.2451/2016PM655.
[166] Lesci IG, Balducci G, Pierini F, Soavi F, Roveri N. Surface features and thermal stability of mesoporous Fe doped geoinspired synthetic chrysotile nanotubes. Microporous Mesoporous Mater 2014;197:8–16. https://doi.org/10.1016/j.micromeso.2014.06.002.
[167] David SR, Geoffroy VA. A review of asbestos bioweathering by siderophore-producing pseudomonas: A potential strategy of bioremediation. Microorganisms 2020;8:1–16. https://doi.org/10.3390/microorganisms8121870.
[168] Foresti E, Gazzano M, Gualtieri AF, Lesci IG, Lunelli B, Pecchini G, et al. Determination of low levels of free fibres of chrysotile in contaminated soils by X-ray diffraction and FTIR spectroscopy. Anal Bioanal Chem 2003;376:653–8. https://doi.org/10.1007/s00216-003-1965-3.
[169] Sprynskyy M, NiedojadŁo J, Buszewski B. Structural features of natural and acids modified chrysotile nanotubes. J Phys Chem Solids 2011;72:1015–26. https://doi.org/10.1016/j.jpcs.2011.05.013.
[170] Schwanke AJ, Lopes CW, Pergher SBC. Synthesis of Mesoporous Material

from Chrysotile-Derived Silica. Mater Sci Appl 2013;04:68–72. https://doi.org/10.4236/msa.2013.48a009.
[171] Lourenço MP, De Oliveira C, Oliveira AF, Guimarães L, Duarte HA. Structural, electronic, and mechanical properties of single-walled chrysotile nanotube models. J Phys Chem C 2012;116:9405–11. https://doi.org/10.1021/jp301048p.
[172] Voitylov V V., Voitylov A V., Korytkova EN, Romanov VP, Ul'yanov S V., Gusarov V V. Structure of aqueous dispersions of Mg3Si2O5(OH)4 nanotubes. Russ J Appl Chem 2008;81:207–11. https://doi.org/10.1134/s1070427208020092.
[173] López-Salinas E, Toledo-Antonio JA, Manríquez ME, Sánchez-Cantú M, Cruz Ramos I, Hernández-Cortez JG. Synthesis and catalytic activity of chrysotile-type magnesium silicate nanotubes using various silicate sources. Microporous Mesoporous Mater 2019;274:176–82. https://doi.org/10.1016/j.micromeso.2018.07.041.
[174] Zhang H, Duan T, Zhu W, Yao WT. Natural Chrysotile-Based Nanowires Decorated with Monodispersed Ag Nanoparticles as a Highly Active and Reusable Hydrogenation Catalyst. J Phys Chem C 2015;119:21465–72. https://doi.org/10.1021/acs.jpcc.5b05450.
[175] Ozeki S, Uchiyama H, Katada M. Hydrolysis of Iron Ion in Chrysotile Nanotubules: A Template Effect on Crystal Growth. Langmuir 1994;10:923–8. https://doi.org/10.1021/la00015a051.
[176] Peng Q, Dai Y, Liu K, Tang X, Zhou M, Zhang Y, et al. Outstanding catalytic performance of metal-free peroxymonosulfate activator: Important role of chrysotile. Sep Purif Technol 2022;287:120526. https://doi.org/10.1016/j.seppur.2022.120526.
[177] Nakagaki S, Castro KADF, Machado GS, Halma M, Drechsel SM, Wypych F. Catalytic activity in oxidation reactions of anionic iron(III) porphyrins immobilized on raw and grafted chrysotile. J Braz Chem Soc 2006;17:1672–8. https://doi.org/10.1590/S0103-50532006000800027.
[178] Chen H, Wan K, Zheng F, Zhang Z, Zhang Y, Long D. Mechanism insight into photocatalytic conversion of lignin for valuable chemicals and fuels production: A state-of-the-art review. Renew Sustain Energy Rev 2021;147:111217. https://doi.org/10.1016/j.rser.2021.111217.
[179] Lang X, Chen X, Zhao J. Heterogeneous visible light photocatalysis for selective organic transformations. Chem Soc Rev 2014;43:473–86. https://doi.org/10.1039/c3cs60188a.
[180] Pouthika K, Madhumitha G. A Mini Review on Recent Advancements in Metal Oxide Integrated Nano-Tubular Inorganic Clay Mineral Photocatalyst for Organic Pollutant Degradation. Comments Inorg Chem 2024;00:1–33. https://doi.org/10.1080/02603594.2024.2312395.
[181] Li Y, Yuan X, Jiang L, Dai H, Zhao Y, Guan X, et al. Manipulation of the halloysite clay nanotube lumen for environmental remediation: a review. Environ Sci Nano 2022;9:841–66. https://doi.org/10.1039/d1en01032h.
[182] Liu J, Zhang G. Recent advances in synthesis and applications of clay-based photocatalysts: A review. Phys Chem Chem Phys 2014;16:8178–92. https://doi.org/10.1039/c3cp54146k.
[183] Jing G, Sun Z, Ye P, Wei S, Liang Y. Clays for heterogeneous photocatalytic decolorization of wastewaters contaminated with synthetic dyes: A review. Water Pract Technol 2017;12:432–43. https://doi.org/10.2166/wpt.2017.046.
[184] Zou Y, Hu Y, Shen Z, Yao L, Tang D, Zhang S, et al. Application of

aluminosilicate clay mineral-based composites in photocatalysis. J Environ Sci (China) 2022;115:190–214. https://doi.org/10.1016/j.jes.2021.07.015.
[185] Papoulis D. Halloysite based nanocomposites and photocatalysis: A Review. Appl Clay Sci 2019;168:164–74. https://doi.org/10.1016/j.clay.2018.11.009.
[186] Imgharn A, Anchoum L, Hsini A, Naciri Y, Laabd M, Mobarak M, et al. Effectiveness of a novel polyaniline@Fe-ZSM-5 hybrid composite for Orange G dye removal from aqueous media: Experimental study and advanced statistical physics insights. Chemosphere 2022;295. https://doi.org/10.1016/j.chemosphere.2022.133786.
[187] Bhatia D, Sharma NR, Singh J, Kanwar RS. Biological methods for textile dye removal from wastewater: A review. Crit Rev Environ Sci Technol 2017;47:1836–76. https://doi.org/10.1080/10643389.2017.1393263.
[188] Katheresan V, Kansedo J, Lau SY. Efficiency of various recent wastewater dye removal methods: A review. J Environ Chem Eng 2018;6:4676–97. https://doi.org/10.1016/j.jece.2018.06.060.
[189] Hsini A, Naciri Y, Bouziani A, Aarab N, Essekri A, Imgharn A, et al. Polyaniline coated tungsten trioxide as an effective adsorbent for the removal of orange G dye from aqueous media. RSC Adv 2021;11:31272–83. https://doi.org/10.1039/d1ra04135e.
[190] Ali H, Ahmed S, Hsini A, Kizito S, Naciri Y, Djellabi R, et al. Adsorption/desorption characteristics of novel Fe3O4 impregnated N-doped biochar (Fe3O4@N/BC) for arsenic (III and V) removal from aqueous solution: Insight into mechanistic understanding and reusability potential. Arab J Chem 2022:104209. https://doi.org/10.1016/j.arabjc.2022.104209.
[191] Brini L, Hsini A, Naciri Y, Bouziani A, Ajmal Z, H'Maida K, et al. Synthesis and characterization of arginine-doped heliotrope leaves with high clean-up capacity for crystal violet dye from aqueous media. Water Sci Technol 2021;84:2265–77. https://doi.org/10.2166/wst.2021.446.
[192] Sudarjanto G, Keller-Lehmann B, Keller J. Optimization of integrated chemical-biological degradation of a reactive azo dye using response surface methodology. J Hazard Mater 2006;138:160–8. https://doi.org/10.1016/j.jhazmat.2006.05.054.
[193] Naciri Y, Ahdour A, Benhsina E, Hamza MA, Bouziani A, Hsini A, et al. Ba3(PO4)2 Photocatalyst for Efficient Photocatalytic Application. Glob Challenges 2023;3:1–11. https://doi.org/10.1002/gch2.202300257.
[194] Wu D, Li J, Guan J, Liu C, Zhao X, Zhu Z, et al. Improved photoelectric performance via fabricated heterojunction g-C3N4/TiO2/HNTs loaded photocatalysts for photodegradation of ciprofloxacin. J Ind Eng Chem 2018;64:206–18. https://doi.org/10.1016/j.jiec.2018.03.017.
[195] Li X, Zhu W, Yan X, Lu X, Yao C, Ni C. Hierarchical La0.7Ce0.3FeO3/halloysite nanocomposite for photocatalytic degradation of antibiotics. Appl Phys A Mater Sci Process 2016;122:1–5. https://doi.org/10.1007/s00339-016-0240-3.
[196] Jatav S, Xiang H, Herber M, Paineau E, Hill EH. In2S3 Growth Templated by Aluminogermanate Double-Walled Imogolite Nanotubes Toward Efficient Visible Light Photocatalysts. Sol RRL 2023;7:3–8. https://doi.org/10.1002/solr.202200947.
[197] Zhang Y, Yang H. Co 3O 4 nanoparticles on the surface of halloysite nanotubes. Phys Chem Miner 2012;39:789–95. https://doi.org/10.1007/s00269-012-0533-9.
[198] Peng H, Wu D, Wan H, Jia LL, Chen G, Li J, et al. Facile synthesis and

characterization of halloysite@W18O49 nanocomposite with enhanced photocatalytic properties. Appl Clay Sci 2019;183. https://doi.org/10.1016/j.clay.2019.105319.
[199] Peng H, Zhang D, Liu X, Tang W, Wan H, Xiong H, et al. Facile synthesis and characterization of core-shell structured Ag3PO4@Hal nanocomposites for enhanced photocatalytic properties. Appl Clay Sci 2017;141:132–7. https://doi.org/10.1016/j.clay.2017.02.023.
[200] Christoforidis KC, Melchionna M, Montini T, Papoulis D, Stathatos E, Zafeiratos S, et al. Solar and visible light photocatalytic enhancement of halloysite nanotubes/g-C3N4 heteroarchitectures. RSC Adv 2016;6:86617–26. https://doi.org/10.1039/c6ra15581b.
[201] Krasilin AA, Bodalyov IS, Malkov AA, Khrapova EK, Maslennikova TP, Malygin AA. On an adsorption/photocatalytic performance of nanotubular Mg3Si2O5(OH)4/TiO2 composite. Nanosyst Physics, Chem Math 2018:410–6. https://doi.org/10.17586/2220-8054-2018-9-3-410-416.
[202] Bahadori E, Vaiano V, Esposito S, Armandi M, Sannino D, Bonelli B. Photo-activated degradation of tartrazine by H2O2 as catalyzed by both bare and Fe-doped methyl-imogolite nanotubes. Catal Today 2018;304:199–207. https://doi.org/10.1016/j.cattod.2017.08.003.
[203] Szczepanik B, Rogala P, Słomkiewicz PM, Banaś D, Kubala-Kukuś A, Stabrawa I. Synthesis, characterization and photocatalytic activity of TiO2-halloysite and Fe2O3-halloysite nanocomposites for photodegradation of chloroanilines in water. Appl Clay Sci 2017;149:118–26. https://doi.org/10.1016/j.clay.2017.08.016.
[204] Nyankson E, Kumar R V. Removal of water-soluble dyes and pharmaceutical wastes by combining the photocatalytic properties of Ag3PO4 with the adsorption properties of halloysite nanotubes. Mater Today Adv 2019;4. https://doi.org/10.1016/j.mtadv.2019.100025.
[205] Guan J, Li J, Ye Z, Wu D, Liu C, Wang H, et al. La2O3 media enhanced electrons transfer for improved CeVO4 @halloysite nanotubes photocatalytic activity for removing tetracycline. J Taiwan Inst Chem Eng 2019;96:281–98. https://doi.org/10.1016/j.jtice.2018.10.030.
[206] Cheng ZL, Sun W. Preparation and Solar Light Photocatalytic Activity of N-Doped TiO2-Loaded Halloysite Nanotubes Nanocomposites. J Mater Eng Perform 2015;24:4090–5. https://doi.org/10.1007/s11665-015-1699-3.
[207] Nyankson E, Agyei-Tuffour B, Annan E, Yaya A, Mensah B, Onwona-Agyeman B, et al. Ag2CO3-halloysite nanotubes composite with enhanced removal efficiency for water soluble dyes. Heliyon 2019;5. https://doi.org/10.1016/j.heliyon.2019.e01969.
[208] Xing W, Ni L, Huo P, Lu Z, Liu X, Luo Y, et al. Preparation high photocatalytic activity of CdS/halloysite nanotubes (HNTs) nanocomposites with hydrothermal method. Appl Surf Sci 2012;259:698–704. https://doi.org/10.1016/j.apsusc.2012.07.102.
[209] Xu J, Zhang B, Jia L, Bi N, Zhao T. Metal-enhanced fluorescence detection and degradation of tetracycline by silver nanoparticle-encapsulated halloysite nano-lumen. J Hazard Mater 2020;386. https://doi.org/10.1016/j.jhazmat.2019.121630.
[210] Wu H, Jian W, Zhang L, Lin J, Li J. Boosting carrier separation in Ag/AgBr/halloysite-nanotubes composites for enhanced photocatalytic performance. Mater Sci Semicond Process 2021;121. https://doi.org/10.1016/j.mssp.2020.105373.

[211] Zou M, Du M, Zhu H, Xu C, Fu Y. Green synthesis of halloysite nanotubes supported Ag nanoparticles for photocatalytic decomposition of methylene blue. J Phys D Appl Phys 2012;45. https://doi.org/10.1088/0022-3727/45/32/325302.
[212] Xing W, Ni L, Liu X, Luo Y, Lu Z, Yan Y, et al. Effect of metal ion (Zn2+, Bi3+, Cr3+, and Ni2+)-doped CdS/halloysite nanotubes (HNTs) photocatalyst for the degradation of tetracycline under visible light. Desalin Water Treat 2015;53:794–805. https://doi.org/10.1080/19443994.2013.844082.
[213] Wang H, Wu D, Li X, Huo P. Ce doping TiO2/halloysite nanotubes photocatalyst for enhanced electrons transfer and photocatalytic degradation of Tetracycline. J Mater Sci Mater Electron 2019;30:19126–36. https://doi.org/10.1007/s10854-019-02268-y.
[214] Jiang L, Huang Y, Liu T. Enhanced visible-light photocatalytic performance of electrospun carbon-doped TiO2/halloysite nanotube hybrid nanofibers. J Colloid Interface Sci 2015;439:62–8. https://doi.org/10.1016/j.jcis.2014.10.026.
[215] Li C, Zhou T, Zhu T, Li X. Enhanced visible light photocatalytic activity of polyaniline-crystalline TiO2-halloysite composite nanotubes by tuning the acid dopant in the preparation. RSC Adv 2015;5:98482–91. https://doi.org/10.1039/c5ra20024e.
[216] Zheng P, Du Y, Chang PR, Ma X. Amylose-halloysite-TiO 2 composites: Preparation, characterization and photodegradation. Appl Surf Sci 2015;329:256–61. https://doi.org/10.1016/j.apsusc.2014.12.158.
[217] Gesesse GD, Le Neel T, Cui Z, Bachelier G, Remita H, Colbeau-Justin C, et al. Plasmonic core-shell nanostructure as an optical photoactive nanolens for enhanced light harvesting and hydrogen production. Nanoscale 2018;10:20140–6. https://doi.org/10.1039/c8nr07475e.
[218] Hojamberdiev M, Khan MM, Kadirova Z, Kawashima K, Yubuta K, Teshima K, et al. Synergistic effect of g-C3N4, Ni(OH)2 and halloysite in nanocomposite photocatalyst on efficient photocatalytic hydrogen generation. Renew Energy 2019;138:434–44. https://doi.org/10.1016/j.renene.2019.01.103.
[219] Lu J, Lin H, Hong R, Zhang D. Photocatalytic H2 evolution properties of K0.5Na0.5NbO3 (KNN) with halloysite nanotubes. Opt Mater (Amst) 2022;129. https://doi.org/10.1016/j.optmat.2022.112516.
[220] Jimenéz-Calvo P, Naciri Y, Sobolewska A, Isaacs M, Zhang Y, Leforestier A, et al. Ti-Modified Imogolite Nanotubes as Promising Photocatalyst 1D Nanostructures for H2 Production. Small Methods 2023;2301369:1–10. https://doi.org/10.1002/smtd.202301369.
[221] Lin S, Zhang Y, You Y, Zeng C, Xiao X, Ma T, et al. Bifunctional Hydrogen Production and Storage on 0D–1D Heterojunction of Cd0.5Zn0.5S@Halloysites. Adv Funct Mater 2019;29. https://doi.org/10.1002/adfm.201903825.
[222] Lasek J, Yu YH, Wu JCS. Removal of NOx by photocatalytic processes. J Photochem Photobiol C Photochem Rev 2013;14:29–52. https://doi.org/10.1016/j.jphotochemrev.2012.08.002.
[223] Ângelo J, Andrade L, Madeira LM, Mendes A. An overview of photocatalysis phenomena applied to NOx abatement. J Environ Manage 2013;129:522–39. https://doi.org/10.1016/j.jenvman.2013.08.006.
[224] Papoulis D, Komarneni S, Nikolopoulou A, Tsolis-Katagas P, Panagiotaras D, Kacandes HG, et al. Palygorskite- and Halloysite-TiO2 nanocomposites: Synthesis and photocatalytic activity. Appl Clay Sci 2010;50:118–24. https://doi.org/10.1016/j.clay.2010.07.013.

[225] Papoulis D, Komarneni S, Panagiotaras D, Stathatos E, Christoforidis KC, Fernández-García M, et al. Three-phase nanocomposites of two nanoclays and TiO2: Synthesis, characterization and photacatalytic activities. Appl Catal B Environ 2014;147:526–33. https://doi.org/10.1016/j.apcatb.2013.09.025.
[226] Laxma Reddy PV, Kavitha B, Kumar Reddy PA, Kim KH. TiO2-based photocatalytic disinfection of microbes in aqueous media: A review. Environ Res 2017;154:296–303. https://doi.org/10.1016/j.envres.2017.01.018.
[227] Cai Y, Sun T, Li G, An T. Traditional and Emerging Water Disinfection Technologies Challenging the Control of Antibiotic-Resistant Bacteria and Antibiotic Resistance Genes. ACS ES&T Eng 2021;1:1046–64. https://doi.org/10.1021/acsestengg.1c00110.
[228] Pichel N, Vivar M, Fuentes M. The problem of drinking water access: A review of disinfection technologies with an emphasis on solar treatment methods. Chemosphere 2019;218:1014–30. https://doi.org/10.1016/j.chemosphere.2018.11.205.
[229] Ipek Yucelen G, Connell RE, Terbush JR, Westenberg DJ, Dogan F. Synthesis and immobilization of silver nanoparticles on aluminosilicate nanotubes and their antibacterial properties. Appl Nanosci 2016;6:607–14. https://doi.org/10.1007/s13204-015-0467-x.
[230] Geraldo DA, Arancibia-Miranda N, Villagra NA, Mora GC, Arratia-Perez R. Synthesis of CdTe QDs/single-walled aluminosilicate nanotubes hybrid compound and their antimicrobial activity on bacteria. J Nanoparticle Res 2012;14. https://doi.org/10.1007/s11051-012-1286-6.